ACHIEVING SIMULTANEOUS REDUCTION OF ROTORCRAFT VIBRATION AND NOISE USING SIMULATION

Dan Patt Li Liu Peretz P. Friedmann

Department of Aerospace Engineering
University of Michigan, Ann Arbor, Michigan, USA

Abstract

A study of the combined helicopter noise and vibration reduction problem was conducted. A fully coupled aeroelastic and aeroacoustic simulation tool is developed, with special attention placed on enhancing the resolution of the free wake model used. Subsequently, this tool is validated with experimental aerodynamic and acoustic data. Control algorithms for noise and vibration problems are studied. The simulation is used to conduct a detailed study of noise and vibration reduction problems in heavy blade-vortex interaction descent flight. Actively-controlled flaps are used to reduce noise and vibrations, and changes to the aerodynamic environment around the rotor is monitored. Simultaneous reduction of noise and vibration is successfully implemented with a dual active flap configuration. Physical sources of increased vibration during noise reduction, and increased vibration during noise reduction are examined, and the power required to reduce noise and vibration is compared to baseline rotor power. The effects of active control on rotor trim are also considered.

Nomenclature

C_N	Sectional normal force coefficient
C_T	Rotor thrust coefficient
C_{d0}	Blade drag coefficient in flow
C_{m0}	Blade moment coefficient in flow
c	Blade chord
$\mathbf{D}$	Matrix defined to be $\mathbf{T}^T\mathbf{Q}\mathbf{T}+\mathbf{R}$
$F_{HX4}, F_{HY4}, F_{HZ4}$	Nondimensional 4/rev hub shears
$J(\mathbf{z}_k, \mathbf{u}_k)$	Objective function
g	Gravitational acceleration
k	Control update index
L_c	Control surface spanwise dimension
M	Local mach number
M_δ	Control surface hinge moment
$M_{HX4}, M_{HY4}, M_{HZ4}$	Nondimensional 4/rev hub moments
$N_{H06}, \ldots, N_{H17}$	Noise levels (in dB) of the 6^{th} - 17^{th} harmonics of blade passage frequency.
N_b	Number of rotor blades
N	Number of flap deflection input harmonic
P_{cs}	Control system power, averaged over one rotor revolution
$\mathbf{Q}$	Weighting matrix for objectives to be reduced
$\mathbf{R}$	Weighting matrix on control input
$\mathbf{r}_I$	Location of start of negative blade loading
r	Distance from rotor hub
R	Rotor radius
$\mathbf{T}$	Sensitivity, transfer matrix between control inputs and objective function
$\mathbf{u}_k$	Control input vector
$\mathbf{u}_{k,\text{opt}}$	Optimum value of control input vector
x_c	Spanwise location of center of control surface
X_{FA}, Z_{FA}	Longitudinal and vertical offsets between rotor hub and helicopter aerodynamic center
X_{FC}, Z_{FC}	Longitudinal and vertical offsets between rotor hub and helicopter center of gravity
$\mathbf{z}_k$	Objective vector
α	Rotor tip-path plane angle relative to tunnel streamwise axis, positive for backward tilt
α_s	Rotor shaft angle
α'	Effective rotor tip-path plane angle α, corrected for wind tunnel effects
α_R	Relaxation coefficient for control algorithm

Presented at the 30th European Rotorcraft Forum, Marseille, France, September 14-16, 2004. *Copyright ©2004 by the authors. All rights reserved.*

δ	Flap deflection angle
ϕ_R	Lateral roll angle
Γ	Blade bound circulation
Γ_I	Inboard peak of blade bound circulation
Γ_O	Outboard peak of blade bound circulation
μ	Helicopter advance ratio
θ_0,θ_{1c},θ_{1s}	Collective and cyclic pitch components
θ_{0t}	Tail rotor cyclic
θ_{tw}	Built-in twist angle
θ_c	Amplitude of pitch control input in HART test
σ	Rotor solidity
ψ_c	Control input phase
ψ	Rotor azimuth angle
ω_{F1}, ω_{L1}, ω_{T1}	Rotating fundamental blade frequencies in flap, lead-lag and torsion, respectively, nondimensionalized with respect to Ω.
Ω	Rotor angular speed

Introduction

Specifications for noise and vibration levels in rotorcraft have increased in stringency, motivated by the desire for smooth ride in helicopters combined with the goal of improving the community acceptance of rotorcraft in densely populated areas. All new helicopters must meet demanding FAA flyover noise level tests, and desirable vibration levels have been identified to be below $0.05g$. Furthermore, active noise and vibration reduction systems must be implemented without undue performance penalties, so as to reap the largest potential benefit on the fairly sizeable cost associated with installing such active control systems in rotorcraft. While these statements apply primarily to civilian operations, similar demands for military operation are driven by pilot fatigue, maintenance costs, weapon system accuracy and the reduction of the noise footprint for stealth purposes.

These requirements have motivated a significant body of research on active vibration reduction (Refs. 1 and 2) as well as noise reduction (Ref. 3). Noise and vibration generation are intrinsically linked as they are fundamentally driven by the same phenomena — unsteady aerodynamic loading and blade motion. Despite these common origins, however, the simultaneous noise and vibration generation/reduction problem is not well understood.

Objectives

The overall objective of this paper is to study combined noise and vibration reduction and investigate the physical processes that frequently cause these objectives to appear mutually exclusive. The specific objectives of this paper are:

1. Describe additional refinements to a coupled aeroelastic/aeroacoustic simulation tool, emphasizing the improvements introduced in the wake model.
2. Present a fairly extensive validation study with HART experimental data.
3. Describe control strategies for noise and vibration reduction
4. Use the simulation to determine the mutual interaction between noise and vibration reduction
5. Study simultaneous noise and vibration reduction using actively controlled flaps (ACFs), implemented in both single and dual flap configurations.
6. Examine the effect of active control on rotor trim.

Achieving these goals will constitute an important contribution towards understanding and attaining simultaneous noise and vibration reduction.

Background

Blade-Vortex Interaction

Blade-vortex interaction (BVI) occurs when a blade encounters the concentrated vorticity trailed by another blade. This phenomenon is usually associated with low speed ($\mu \approx 0.15$) descending flight, when the trailed rotor wake is closely spaced and likely to lie largely in the plane of the rotor. The interaction generates large unsteady pressure fluctuations on the blade that produce high levels of vibration and noise. The vibration levels often exceed those present at higher advance ratios ($\mu \approx 0.30$) in level flight. The noise generated by BVI has several distinctive characteristics. It tends to have a strong directivity pattern focused mostly forward and under the rotor plane (Ref. 3), making it particularly apparent to an observer on the ground ahead of a descending helicopter. The noise is also very periodic, with a frequency content typically defined to be the 6^{th} through 40^{th} harmonics of blade passage frequency, in the mid-frequency range, generally considered to be most annoying to human

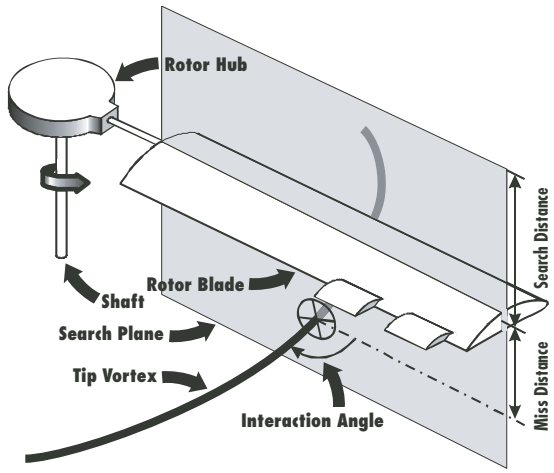


Figure 1: *BVI Intersection showing miss distance and interaction angle*

hearing. Figure 1 depicts a typical blade-vortex interaction and defines the properties of miss-distance and interaction angle.

There are a number of factors governing BVI events:

1. The advance ratio, rate of descent, and rotor angular speed all affect the geometry of the trailed wake, and thus the strength and type of BVI. Noise from BVI is most severe when the wake is trailed directly into the plane of the rotor and oncoming blades.

2. The magnitude of pressure fluctuations on the rotor blade have a strong effect on the magnitude of BVI noise and vibration produced. Subsequently, circulation strength and trajectory of the vortex segment may be influenced.

3. The miss distance between a vortex segment and the oncoming rotor blade can enhance a BVI event as the miss distance becomes smaller

4. The interaction angle between the vortex segment and blade in the plane of the rotor (whether an interaction is parallel or not) can alter both the magnitude of BVI noise and the propagation efficiency.

Active control has the potential to mitigate BVI noise and vibration by modifying any of the three characteristics affecting BVI strength: pressure fluctuations, miss distance or interaction angle.

Approaches to Vibration and Noise Reduction

Both active and passive techniques have been developed for vibration and noise reduction, and it is likely that the best rotor could benefit from a judicious combination of these two techniques. However, this paper will focus on active techniques. A number of active control approaches, illustrated schematically in Fig. 2, have been developed for vibration reduction (Ref. 1). These fall into one of two categories: (a) active control approaches aimed at reducing vibrations in the rotor before they propagate into the fuselage, and (b) active control approaches implemented in the fuselage using an approach known as active control of structural response (ACSR). Within the first category of active control, where the primary objective is to reduce vibrations in the rotor, two approaches have emerged. These are (1) higher harmonic control (HHC) where the blades are activated in the nonrotating swashplate by introducing pitch commands, and (2) individual blade control (IBC) where each blade can be controlled independently in the rotating frame. Several implementations of IBC are available: (i) the conventional or earliest implementation based on pitch actuation at the blade root in the rotating system, (ii) actively controlled partial-span trailing-edge flaps, and (iii) the active-twist rotor where the entire blade is twisted by piezoelectric fiber embedded in the blade. Additional descriptions of these approaches can be found in Refs. 2 and 4.

During the last decade, the HHC and IBC approaches, developed primarily for vibration reduction, have also been considered as a means of reducing BVI noise. However, the control algorithms used are essentially the same as those devised for vibration reduction, and no attempts were made to develop special algorithms for the noise reduction problem.

The Simultaneous Problem

Several experimental studies have been conducted where control techniques have been used in wind tunnel tests to reduce vibrations and noise. Most of these studies have been performed in the open-loop mode, and have demonstrated noise and vibration reduction. The reduction of the desired quantity was accomplished through a careful selection of a harmonic pitch command and its phase angle in the open-loop mode. Highlights of these results are summarized in Table 1.

It has been noted in previous studies that the control inputs that reduce noise tend to increase vibration and vice-versa for both HHC (Refs. 5, 7) and IBC (Refs. 6, 8, 9). A recent test using the active twist rotor (ATR) has produced similar findings (Ref. 10). Although both vibrations and noise are due to BVI phenomena, the harmonic control inputs required for noise or vibration reduction are often quite different. It is interesting to note that Table 1 lists three instances of simultaneous reduction, denoted as (*ii*), (*v*) and (*vii*). Each of

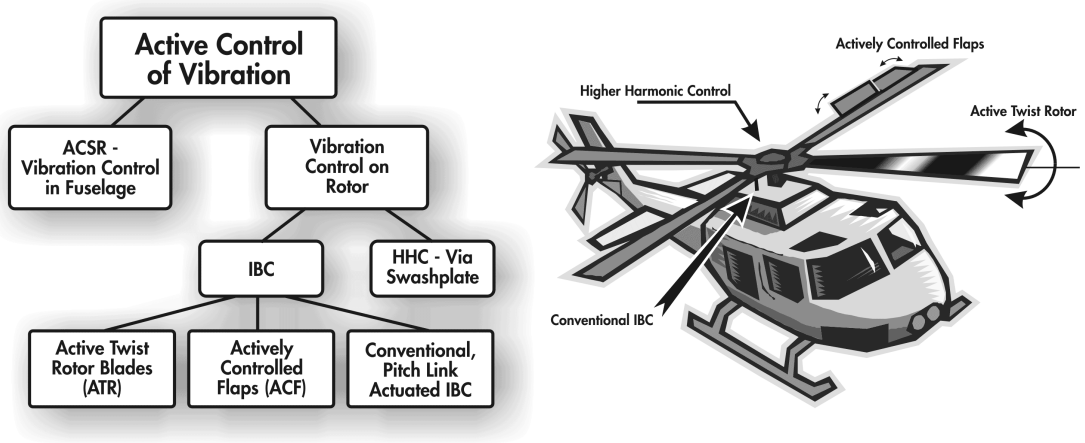


Figure 2: *Overview of Active Control Approaches*

No.	Ref.	Test Year	Rotor Type	Type	Freq.	Phase	Vibration % Change	Noise dB Change
i	(Ref. 5)	1989	ARES†	HHC	$4/rev$	60°	+100	-4
ii	(Ref. 6)	1994	BO-105	IBC	$2/rev$	60°	-20	-5
iii	”	”	”	”	$3/rev$	315°	+130	-5
iv	”	”	”	”	$4/rev$	90°	+35	-2.5
v	”	”	”	”	$2+5/rev$	$60^{\circ}+90^{\circ}$	-80	-8
vi	(Ref. 7)	1994	BO-105†	HHC	$3/rev$	30°	+60	-4
vii	”	”	”	”	$4/rev$	90°	-10	-3
viii	”	”	”	”	$5/rev$	15°	+600	-2
ix	(Ref. 8)	1998	BO-105‡	IBC	$2/rev$	200°	+50	-6
x	(Ref. 9)	2001	UH-60	IBC	$2/rev$	180°	up to +100	-6 to -12

†Scaled model rotor, ARES: Aeroelastic Rotor Experimental System. ‡Flight test.
*Note: These are approximate results and may not be directly comparable due to differing test conditions, control techniques and metrics for noise and vibration. Refer to the individual references for details.

Table 1: *Concise Summary of Active Control Experiments Measuring Noise and Vibration*

these cases, however, was very sensitive to the control input given, and the degree of reduction achieved was not as significant as other cases of individual vibration or noise reduction. For some of these cases, a small change in control phase of 10° eliminated the simultaneous reduction. For the one multi-harmonic case that achieved a simultaneous reduction (*v*), when the amplitude of the $5/rev$ component was changed by just 0.25° the vibration levels increased from the baseline. Therefore, it is evident that achieving simultaneous reduction of noise and vibration is difficult, and the reasons for success or failure are not well understood.

Computational simulations have also failed to provide satisfactory insight on these experimental results, and attempts to explain the underlying physics have not been successful. The first Higher-harmonic-control Aeroacoustic Rotor Test (HART-I) was conducted in the early 1990s at the German-Dutch Wind Tunnel (DNW)(Refs. 7, 11) and was intended to provide a detailed study of blade vortex interaction (BVI) effects on helicopter rotor blade airloads and noise. A second test, dubbed HART-II (Ref. 12) of an almost identical configuration has also been conducted, providing similar results. In the HART-I test (Ref. 7), it was implied that a change in BVI miss-distance contributed to lowered noise, but other studies suggest that changes in BVI inclination angle are more likely to be responsible for lowered noise (Ref. 13). As implied from this review, further study is required to improve the fundamental understanding of the mechanism of simultaneous vibration and noise reduction.

Two recent papers have focused specifically on the consequences of vibration reduction using actively controlled flaps on noise levels (Ref. 14) and the effects of noise reduction on vibration (Ref. 15). The present paper will combine and extend the research described in the previous papers (Ref. 14, 15).

Description of Model

The present study is based on an aeroelastic response analysis capable of modeling vibration reduction in rotorcraft using single and dual ACF systems. The code, which has been gradually developed by the last author and his students during the last decade, contains an unsteady aerodynamic model capable of unsteady pressure distribution prediction coupled with structural and acoustic modules. Details on the structural, aerodynamic and acoustic models used in the simulation can be found in Refs. 14 and 15. During the validation studies described in this paper, several important modifications had to be made to the free wake routine used in previous simulations that focused exclusively on vibration reduction (Ref. 16).

In describing the model it is relevant to note that there are two approximations in the aerodynamic model. First, the ONERA dynamic stall model that was included in previous studies [17] has been turned off in these studies. This neglect can be justified when dealing with BVI that occurs at low advance ratios ($\mu \approx 0.15$). Next, it should be noted that the aerodynamic influence of the fuselage has been neglected. This may not be a trivial effect; it was shown in Ref. 18 that the presence of a fuselage can effect vibration levels by 20%, and a similar influence on noise might be expected.

Wake Model

The current aeroelastic simulation code is based a number of previous studies (Refs. 16, 17, 19, 20) which have been aimed at active vibration reduction. The free wake model in these codes was based on the CAMRAD/JA (Refs. 21, 22) wake, which is computationally efficient but contains simplifications that caused the model to be incapable of representing the acoustic data obtained in the HART experiments. The principal shortcomings that were identified and corrected in the course of this study are described next.

1. For accurate prediction of BVI noise, a 5° or finer azimuthal wake resolution is required, as compared to the much coarser 15° resolution that is often adopted for vibration reduction studies.

2. The free wake model taken from CAMRAD/JA was predicated on the assumption that the inboard vortices cannot roll up, such that either a vortex-sheet or an equivalent vortex-line model could be used to model the inboard vortices. This was not compatible with HART test data where significant increases in BVI noise levels for the "minimum vibration" (MV) case have been attributed to a dual vortex structure (Ref. 7).

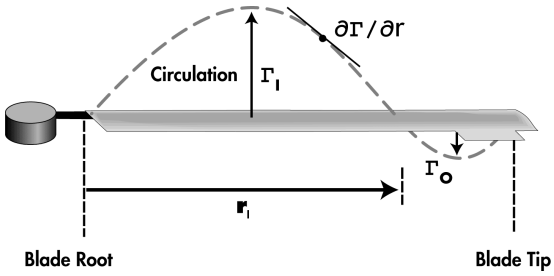


Figure 3: *Blade circulation distribution leading to a dual vortex structure*

Based on these observations, the shortcomings of the free-wake model have been remedied by introducing the changes listed below.

a. The wake code was modified to allow for refined wake resolution of up to 2°. However, under some conditions the free wake model (Ref. 23 failed to converge for this resolution and therefore the smallest resolution in the computation carried out in this paper was $5^\circ$of azimuth.

b. A dual vortex was incorporated by using a second inboard vortex line. This feature of the wake model becomes active only when the tip loading becomes negative, as shown in Fig. 3. The release point of this second vortex line is taken to be at the radial location r_I, where blade bound circulation becomes negative, and the strength of this vortex is assumed to be $\Gamma_I - \Gamma_O$, where Γ_O, the outboard circulation peak, is negative. The free wake distortion computation routine was also modified to include the deformation of this second inboard vortex line, including its interaction with the outer tip vortices taken into account. Induced velocities at both tip vortices and secondary vortices are evaluated to give the final distorted wake geometry. Furthermore, a threshold criteria, suggested in Ref. 24, is introduced to determine whether to have inboard vortex line rolled up. This is accomplished by requiring the radial gradient of the bound circulation $\partial\Gamma/\partial r$ at the inboard vortex release point r_I be greater than a specified threshold value that allows for rollup of the inboard vortex. This represents the physical requirement that the shear in the wake be sufficiently strong so as to form a fully rolled-up, concentrated vortex.

c. An optional viscous core growth model (Ref. 25) was also introduced into the code, which simulates the viscous diffusion of the vortex core with age. However, after extensive testing that employed HART data, there was insufficient evidence to warrant the use of this feature when compared to the conventional constant core vortex model.

Control Algorithm

The higher-harmonic control algorithm is used for both noise and vibration reduction. This algorithm has been the subject of a recent paper (Ref. 26), wherein the stability, robustness, and convergence properties of the algorithm and a number of variants are explored.

The algorithm is based on a linear, quasi-static, frequency domain representation of helicopter response to control inputs. The input harmonics to the ACF consist of a combination of flap deflection angles having frequencies of 2, 3, 4 and $5/rev$. The total flap deflection is a combination of these contributions:

$$\delta(\psi) = \sum_{N=2}^{5} \left[\delta_{Nc}\cos(N\psi) + \delta_{Ns}\sin(N\psi)\right]. \qquad (1)$$

These pitch deflection contributions are related to the vibration or noise level magnitudes through a transfer matrix $\mathbf{T}$, given by

$$\mathbf{T} = \frac{\partial \mathbf{z}_k}{\partial \mathbf{u}_k}. \qquad (2)$$

The control strategy is based on the minimization of a performance index described in Refs. 1, 20, 26 and 27 that is a quadratic function of the quantities that are being reduced (vibration or noise) $\mathbf{z}_k$ and control input amplitudes $\mathbf{u}_k$:

$$J(\mathbf{z}_k, \mathbf{u}_k) = \mathbf{z}_k^{\mathrm{T}}\mathbf{Q}\mathbf{z}_k + \mathbf{u}_k^{\mathrm{T}}\mathbf{R}\mathbf{u}_k, \qquad (3)$$

The subscript k refers to the k^{th} control step, reflecting the discrete-time nature of the control. The time interval between each control step must be sufficient to allow the system to return to the steady state so that the vibration or noise levels can be accurately measured. The optimal control law is given by:

$$\mathbf{u}_{k,\text{opt}} = -\mathbf{D}^{-1}\mathbf{T}^{\mathrm{T}}\{\mathbf{Q}\mathbf{z}_{i-1} - \mathbf{Q}\mathbf{T}\mathbf{u}_{i-1}\} \qquad (4)$$

where

$$\mathbf{D} = \mathbf{T}^{\mathrm{T}}\mathbf{Q}\mathbf{T} + \mathbf{R} \qquad (5)$$

For a well-identified linear system the algorithm converges to the optimum value in a single step (Ref. 26). However, if the helicopter cannot be perfectly represented by a linear model, the optimal value will not be reached after the first step. Using the procedure outlined in Ref. 26, the relaxed version of the HHC algorithm is used in this study. Traditionally, the control input updates could be represented in iterative form as shown in Eq. 6:

$$\mathbf{u}_{\mathrm{k+1}} = \mathbf{u}_{\mathrm{k}} + \Delta\mathbf{u}_{\mathrm{k}}. \qquad (6)$$

In the relaxed variant of the algorithm, a relaxation factor α_R is introduced,

$$\mathbf{u}_{\mathrm{k+1}} = \mathbf{u}_{\mathrm{k}} + \alpha_R\Delta\mathbf{u}_{\mathrm{k}}, \qquad (7)$$

where $0 < \alpha_R < 1$. This has been shown to increase the robustness of the algorithm at the expense of convergence speed (Ref. 26). An adaptive version (Refs. 26, 27) of the HHC algorithm was also useful in some of the noise reduction studies. In the adaptive variant, the transfer matrix $\mathbf{T}$ is identified online, following the method described in Ref. 26.

For vibration reduction (VR) studies, the vector $\mathbf{z}_k$

consists of $4/rev$ vibration levels as shown in Eq. 8,

$$\mathbf{z}_{k,\mathrm{VR}} = \begin{bmatrix} F_{HX4} \\ F_{HY4} \\ F_{HZ4} \\ M_{HX4} \\ M_{HY4} \\ M_{HZ4} \end{bmatrix} \tag{8}$$

For BVI noise reduction (NR), the objective function based on hub shears and moments (Eqs. 3 and 8) is modified by using Eq. 9, instead of Eq. 8 together with Eq. 3.

$$\mathbf{z}_{k,\mathrm{NR}} = \begin{bmatrix} N_{H06} \\ N_{H07} \\ N_{H08} \\ \vdots \\ N_{H17} \end{bmatrix} \tag{9}$$

For noise reduction, the vector $\mathbf{z}_{k,\mathrm{VR}}$ from Eq. 9 includes acoustic pressure levels in the 6^{th}-17^{th} harmonics of blade passage frequency as measured at a microphone installed at a suitable location . As shown in Fig. 4, these locations are usually on the skid or landing gear of the helicopter.

For simultaneous reduction (SR) problems, a combined vector is defined:

$$\mathbf{z}_{k,\mathrm{SR}} = \left[\frac{\mathbf{z}_{k,\mathrm{VR}}}{\mathbf{z}_{k,\mathrm{NR}}} \right]. \tag{10}$$

Where the vector $\mathbf{z}_{k,\mathrm{SR}}$ is simply a partitioned combination of hub shear and noise levels. The weighting matrix $\mathbf{Q}$ is used to adjust the control effort so as to achieve a desirable balance between the vibration and noise reductions levels.

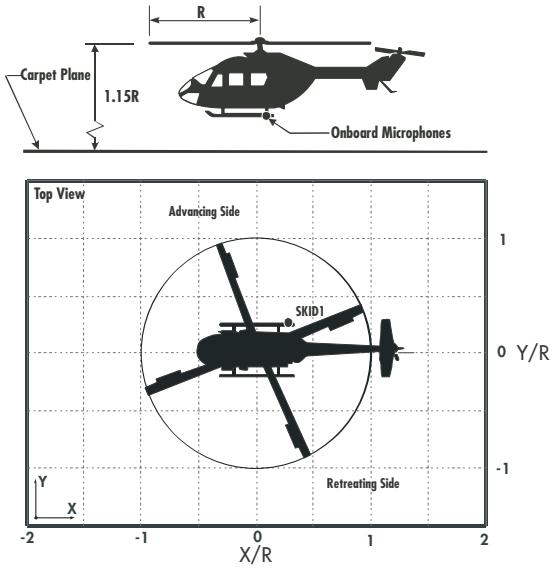


Figure 4: *Microphone locations on and around the helicopter for noise feedback*

For the control problems considered in this paper, two identification techniques were used. First, an off-line identification procedure is used where control inputs are perturbed one at a time, and the effect on the output vector $\mathbf{z}$ is measured (or computed), determining the elements of the sensitivity matrix $\mathbf{T}$ one row at a time. This off-line identification technique, combined with a relaxation factor $\alpha = 0.3 - 0.5$, is referred to as *conventional* HHC in this paper. A second, on-line identification technique, discussed in Ref. 26, is also used, and is referred to as *adaptive* HHC for this study. With this technique, a recursive least-squares technique is used to identify $\mathbf{T}$ in the closed loop.

It is important to emphasize that when the control algorithms described above are used, fairly large flap deflections can be encountered. For operational reasons, during the practical implementation of an ACF system on a helicopter, flap deflections will be usually limited to values that do not exceed $\delta_{fmax} \leq 4^{\circ}$. When such limits are imposed the flap saturates and the vibration reduction capability is lost. To remedy this situation, the algorithm has been modified to account for actuator saturation (Ref. 28). When this modified version of the algorithm is used flap angles can be limited to specified maximum values without encountering a significant loss in control effectiveness. The version of the control algorithm used in the present study contains this particular modification.

Model Validation

The HART test rotor was a 40-percent dynamically and Mach-scaled model of a 4-bladed hingeless MBB BO-105 main rotor, with -8° linear twist and standard rectangular tip shape. The test setup used is depicted in Fig. 5. One of the blades was heavily instrumented with pressure transducers so that blade airloads could be measured at various radial locations. Microphones were placed underneath the rotor hub and moved across the horizontal plane to measure the rotor noise at various locations, which gives the directivity of noise emission. Blade-vortex interaction noise, was comprised of the $6^{\mathrm{th}} - 40^{\mathrm{th}}$ blade passage frequency harmonics of the overall measured acoustic pressure. The rotor was trimmed for a given advance ratio μ, thrust coefficient C_T and rotor shaft angle α_s, using collective and $1/rev$ cyclic pitch inputs. The dataset acquired in this trimmed condition is denoted the *baseline* case. Subsequently, higher harmonic pitch inputs were superimposed through swashplate. This higher harmonic control capability is essential to the HART test, in order to explore the potentials of HHC for the reduction of BVI noise. The swashplate was activated in such a way as to provide $3 - 5/rev$ pitch components in the rotating frame. All control inputs were

introduced in the open-loop mode.

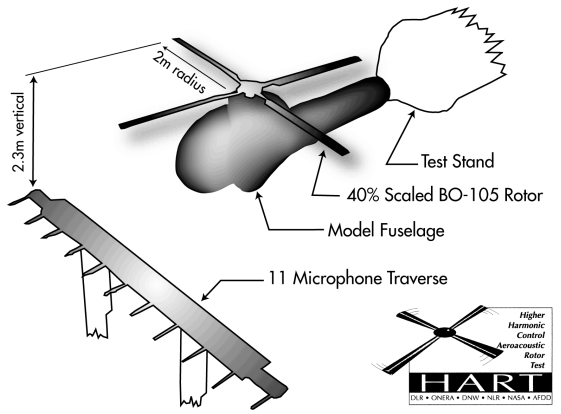


Figure 5: *HART Test Setup*

The baseline HART test case was chosen to simulate typical BVI conditions, with $\mu = 0.15$ and $\alpha_s = 5.3^\circ$, which roughly corresponds to 6.5° descent flight in heavy BVI. This nominal baseline test case (without HHC) is denoted "BL" in the study and related documentation. When the HHC system was engaged, a systematic HHC phase sweep was conducted for $3-5/rev$ components in order to determine the optimal conditions for the reduction of BVI noise and vibration. It was found that $3/rev$ components were most influential for both BVI noise and vibration reduction. The two optimal cases, where BVI noise or vibration levels were most successfully minimized, were achieved by using $3/rev$ control inputs; however, they were applied at different phase angles. These cases are designated the "minimum noise" (MN) case and "minimum vibration" (MV) cases respectively. A maximum of 6dB in BVI noise reduction was observed in MN case. However, it was accompanied by a dramatic increase (nearly 100%) in vibration levels. Similarly, a 30% reduction achieved in MV case was also followed by a 2.5dB increase in the advancing side BVI noise.

The HART project provides an extensive, high quality database for helicopter rotor simulation code validation. It generated important information on rotor aerodynamics, wake structures, aeroelastic blade deformation and acoustics. This extensive experimental database has extraordinary value when attempting to understand and improve helicopter simulation codes. The parameters of HART test are listed in Table 2.

Parameter	Value
N_b	4
σ	0.077
Ω (rpm)	1040
μ	0.15
C_T	0.0044
R (m)	2
c/R	0.0605
θ_{tw}	-8°

Table 2: HART model configuration

HART Case	α_s	α'	θ_c	ψ_c
Baseline (BL)	5.3°	4.1°	none	none
Min. Noise (MN)	5.3°	4.1°	-0.85°	38°
Min. Vibration (MV)	5.3°	4.1°	-0.85°	119°

Table 3: HART test configurations

Comparison of Blade Tip Deformations

In the HART study, the first six rotating natural frequencies corresponding to the first six *uncoupled* (Ref. 11) modes of the model rotor were measured; these values are presented in Table 4. The structural model used in the present simulation (Ref. 15) has fully-coupled flap, lag and torsional dynamics, and discretization is based on the global Galerkin method with three flapping modes, two lead-lag modes and two torsional modes. For the simulation, the structural properties of the blade were chosen to match the uncoupled modal frequencies of the HART study as closely as possible, following the procedure described in Ref. (Ref. 29). Table 4 lists the blade natural frequencies for both the simulation and the HART study. The first five frequencies compare well with measured HART values. A convergence study to determine the effect of including additional modes has not yet been performed.

Mode	HART	Simulation
1st Lead-Lag	0.63	0.73
1st Flapping	1.14	1.11
2nd Flapping	2.63	3.21
1st Torsion	3.89	3.93
2nd Lead-Lag	4.46	4.46
3rd Flapping	4.69	6.90
2nd Torsion	–	11.44

Table 4: Structural data, frequencies in $/rev$

The vertical and torsional tip deformations as predicted by our analysis are compared with HART experimental data (Ref. 11) in Fig. 6. The baseline and MV cases compare reasonably well, but the MN case displays some variations from experimental data. The torsional deflections have an important effect on aerodynamic loads; previous studies (Refs. 30,31) have noted

that using prescribed torsional deformations could significantly enhance correlation. In Fig. 6 it is apparent that the simulated results are slightly off from HART data in both magnitude and phase for the MN and MV cases, while the simulated baseline result shows very little variance over the course of a revolution. Despite these discrepancies with experimental data, the present results compare favorably with previously published work (Ref. 25, 30).

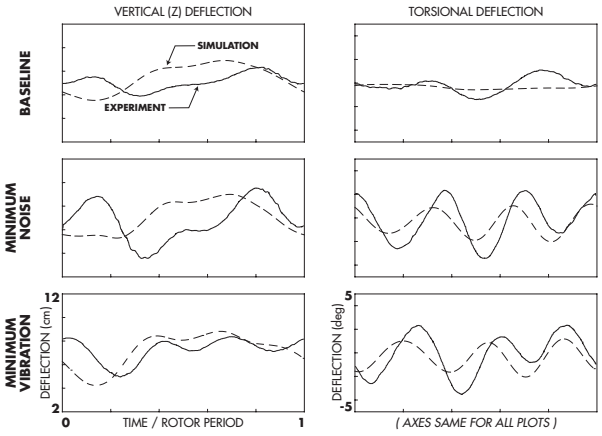


Figure 6: *Comparison of simulated blade deformations with HART measurement*

Aerodynamic Loads

The aerodynamic loads obtained from the simulation and measured in HART test are compared in Fig. 7. The vertical axis in Fig. 7 represents a non-dimensional product of the normal force coefficient and the square of the local mach number. This quantity is measured at a location $r/R = 0.87$ along the span of the blade. These plots can be interpreted to be a superposition of two effects: a larger, low-frequency oscillation, and a series of smaller, high-frequency "spikes". The spikes are pressure variations produced by BVI encounters. The magnitudes of aerodynamic loading measured in the HART test are reproduced with reasonable accuracy by the simulation. In the baseline case, the character of the HART loading is predicted reasonably well, capturing the valley halfway through the revolution. This feature has been noted as particularly difficulty to capture by other validation efforts (Ref. 31).

Wake Geometry and BVI Comparisons

Two comparisons were carried out to validate the modified wake routine against measured HART data. First, the simulated vortex filament geometry was compared with HART laser-light sheet (LLS) data at two azimuthal positions: 35° on the advancing side and 295° on the retreating side. These positions were chosen because they are near the most important BVI interactions. Figure 8 depicts the approximate blade location in the vicinity of several wake segments. The solid lines represent the simulated wake, while the shorter dashed lines are data from the HART test. The results show good agreement only for the baseline and MV cases for the advancing blade. For the MV case, the full dual vortex structure on the advancing side is well captured. The retreating side has worse correlation than the advancing side, perhaps only the baseline case has acceptable correlation. Difficulties with correlating all cases have been noted in other validation efforts (Ref. 32), and therefore only rarely attempted – matching the shape and curvature of vortex segments is difficult even when the location of the wake segments is predicted reasonably well.

The BVI locations as predicted by the present simulation are compared to the results published in Ref. 32 in Fig. 9. Each data point represents the location of an individual blade-vortex interaction event. A number of experimental data points (indicated by triangles) are also included using a procedure described in Ref. 32. These plots show that the current wake model compares generally well against both previous studies and HART data, but that it is difficult to record the all of the interactions on the advancing and retreating sides.

Acoustic Correlation

Comparison of the complete aeroelastic/aeroacoustic simulation capability against HART experimental data is an important ingredient of this validation study. For the HART test, the acoustic environment was measured by traversing a microphone array positioned $1.15R$ below the rotor as shown in Fig. 5. From this data, time-averaged decibel (dB) levels could be computed on a "carpet plane" parallel to and below the rotor, as shown in Fig. 4. The HART baseline case is compared against the simulation in Fig. 10. Overall, excellent agreement is obtained. The magnitudes of the advancing-side and retreating side peaks are predicted exactly. The position of the peaks is also well-predicted, although the retreating-side peak is slightly smaller in the simulation.

The results for the minimum noise (MN) case are given in Fig. 11. It is apparent that the advancing side noise was not well-predicted for this case. However, on the retreating-side, the lobe's location and magnitude are well-predicted. Figure 12 shows the results for the HART minimum vibration (MV) case. The simulation under-predicts the noise levels by $1-3$dB in this case. However, the character of the noise is well captured on both the advancing and retreating sides.

The simulated time history of acoustic pressure is

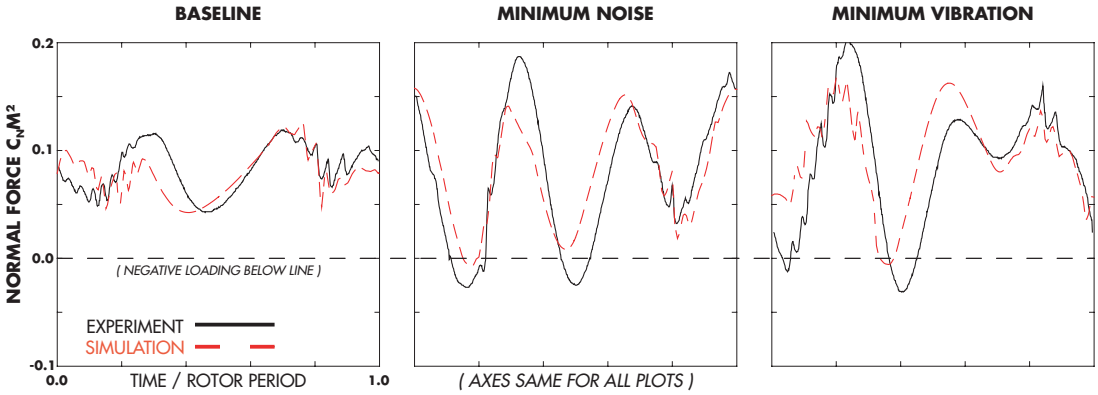


Figure 7: *Comparison of simulated aerodynamic loads with HART data*

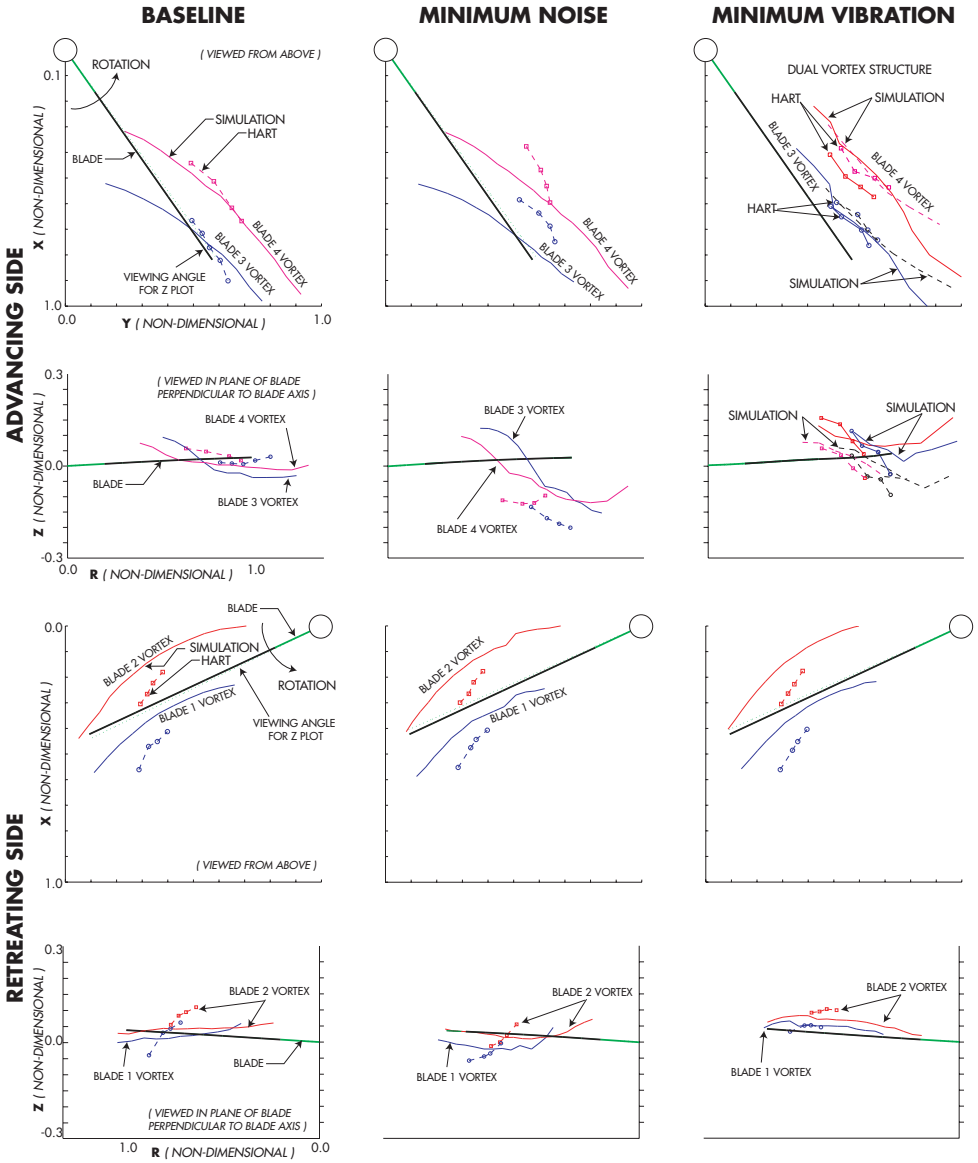


Figure 8: *Validation of wake geometry prediction with HART data*

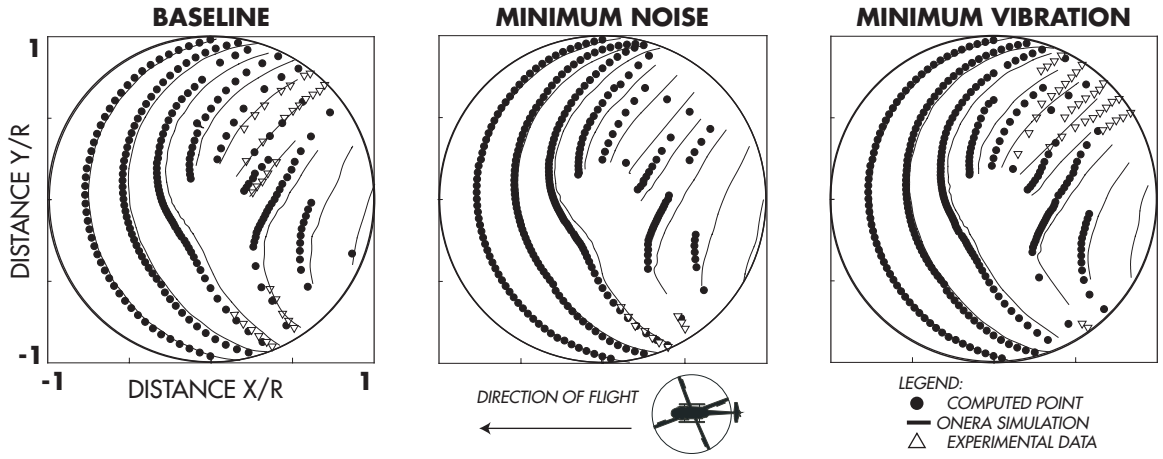


Figure 9: *Validation of BVI interaction predictions with Ref. 32 and HART data*

compared against HART data for the noisiest locations on the advancing and retreating sides is compared in order to obtain further information on the predictive capabilities of the code. Good agreement is evident between simulation and experiment on both the advancing and retreating sides.

The pressure signatures for the minimum noise (MN) case are shown in Fig. 14. Once again, good agreement is obtained for the pressure signature despite the poor results on the advancing side of the carpet plot. The minimum vibration (MV) acoustic pressure signatures are compared in Fig. 15. Excellent agreement is obtained with experimental data in both magnitude and phase of the signature.

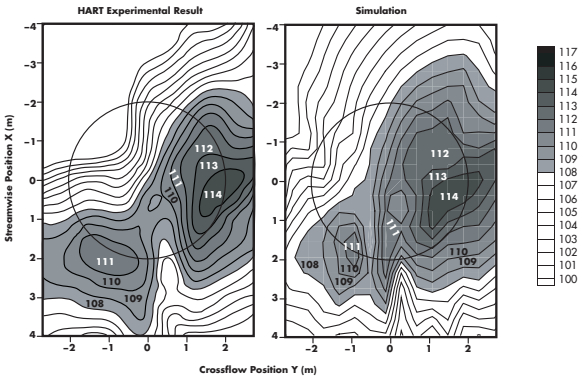


Figure 10: *Acoustic validation of baseline case with HART carpet plot*

Vibration Levels

The simulation code was also used to predict vibratory hub loads for the baseline, MN and MV HART cases, as shown in Fig. 16. The HART vibratory data is not in a form directly comparable to the information presented here, however, it was noted that vibration levels for the MN case are around 100% higher than for the baseline case, a feature well-captured by the simulation.

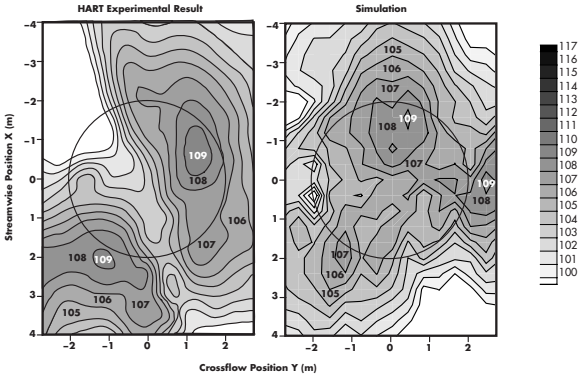


Figure 11: *Acoustic validation of minimum noise case with HART carpet plot*

Results

The results presented in this section were obtained for a helicopter configuration resembling a full-scale MBB BO-105 helicopter with a four-bladed hingeless rotor system. The results are obtained using a propulsive trim procedure that is implemented within a coupled trim/aeroelastic analysis. The data used in the computations is summarized in Table 5. The characteristics of the actively controlled flap configurations are given in Table 6. The acoustic environment in the

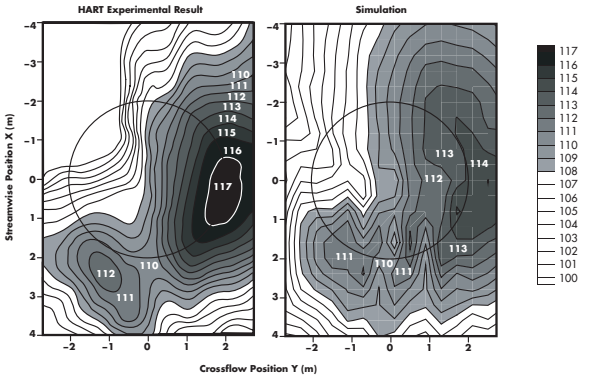


Figure 12: *Acoustic validation of minimum vibration case with HART carpet plot*

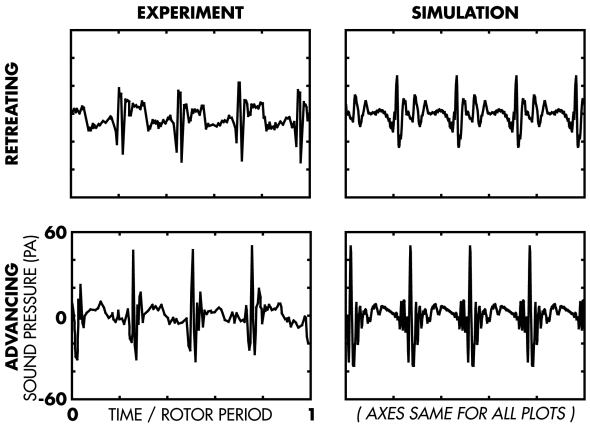


Figure 13: *Advancing and retreating side acoustic pressure signatures compared with HART data for the baseline case*

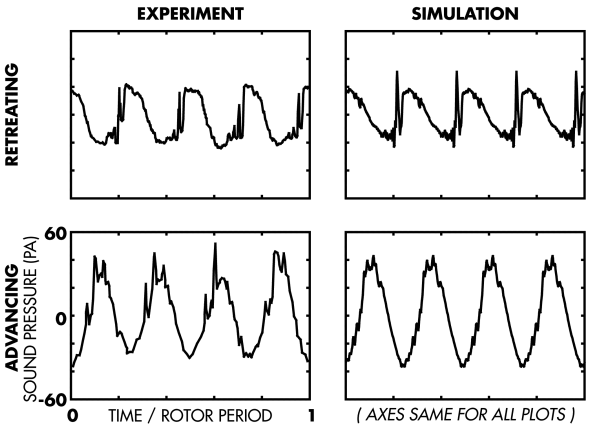


Figure 14: *Advancing and retreating side acoustic pressure signatures compared with HART data for the minimum noise case*

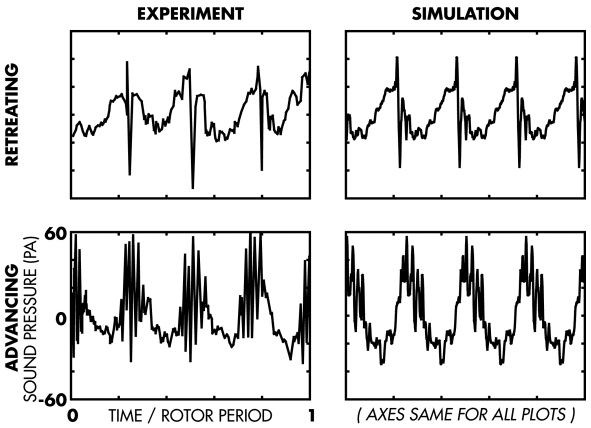


Figure 15: *Advancing and retreating side acoustic pressure signatures compared with HART data for the minimum vibration case*

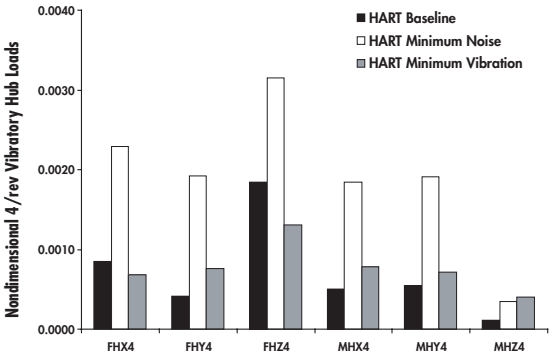


Figure 16: *Simulated 4/rev vibratory hub shears and moments for HART test cases*

vicinity of the helicopter is obtained by assuming that microphones capable of measuring the required noise levels are distributed in a grid on the carpet plane beneath the rotor as depicted in Fig. 4. A feedback microphone is placed on a boom extending from the right landing skid at the rear (labeled SKID1). A flight-test (Ref. 8) has indicated that, for several flight conditions, skid-mounted microphones provide very good correlation with ground-based noise levels. However, other analytical studies have suggested that the near-field to far-field noise radiation pattern may not always be simple (Ref. 33). A previous study (Ref. 15) has suggested that feedback microphones place on the right landing skid (but not on the nose boom) correlate well with advancing side noise levels on a carpet plane below the rotor.

All vibration, noise and simultaneous reduction studies were performed at the same flight condition: a simulated 6.5° descent in heavy BVI at $\mu = 0.15$. In general, both single flap and dual flap configurations are considered in each reduction study.

Rotor Data	
$N_b = 4$	$c = 0.05498 L_b$
$\omega_{F1} = 1.123$	$C_{do} = 0.01$
$\omega_{L1} = 0.732$	$C_{mo} = 0.0$
$\omega_{T1} = 3.17$	$a_o = 2\pi$
$\theta_{tw} = -8^\circ$	$\alpha' = 6^\circ$
$\gamma = 5.5$	$\sigma = 0.07$
2.5° precone angle	
Helicopter Data	
$C_W = 0.005$	$\mu = 0.15$
$X_{FA} = 0.0$	$Z_{FA} = 0.3$
$X_{FC} = 0.0$	$Z_{FC} = 0.3$

Table 5: Elastic blade configuration

$c_c = 0.25c$	
Single Flap	
$x_c = 0.75 L_b$	$L_c = 0.12 L_b$
Dual Flap	
$x_{cs}^1 = 0.72 L_b$	$L_{cs}^1 = 0.06 L_b$
$x_{cs}^2 = 0.92 L_b$	$L_{cs}^2 = 0.06 L_b$

Table 6: Flap configuration

Noise Generation During Vibration Reduction

The conventional HHC control algorithm was used to reduce $4/rev$ vibratory hub loads and moments in both single and dual flap configurations. The resulting vibration levels for these cases are compared with the baseline, uncontrolled result in Fig. 17. It is clear that both flap configurations are effective at reducing vibratory loads, with the single flap reducing the vertical hub shear 69%, while the dual flap is slightly more effective at 79%. When saturation limits are imposed, flap deflections are constrained to remain between $+4^\circ$ and -4°. The dual flap configuration can achieve vibration reduction of 68% with saturation limits imposed, almost as effective as the single flap case, suggesting that this is a viable option.

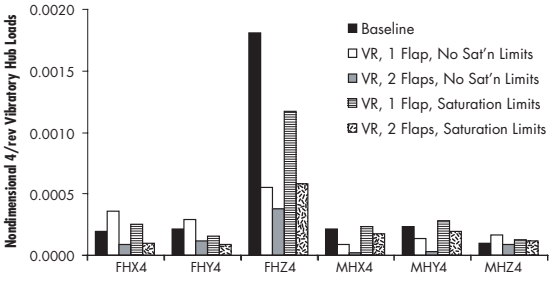


Figure 17: *Vibration levels, vibration reduction with 1 and 2 flaps, full-scale BO-105*

The noise production on a carpet plane below the rotor for the baseline, single flap, and dual flap configurations with and without saturation limits is shown in Fig. 18b-18e. The sound pressure level (SPL) decibel (dB) level is computed with respect to a reference pressure of 20μPa. The noise directivity of the baseline case is characterized by the high noise levels on the advancing and retreating side. After vibration reduction with a single ACF, the noise levels increase by one to two dB as shown in Fig. 18b. The increase is most apparent on the advancing side in the first quadrant, with maximum BVI levels increasing to $116dB$. The retreating side is less affected, and most noise levels remain almost the same. With a dual ACF configuration (Fig. 18c), the acoustic footprint remains almost identical to the baseline case, Fig. 18a. The peaks of maximum noise on the advancing and retreating side shift slightly , but the magnitude of BVI noise remains essentially unchanged. When saturation limits are imposed, shown in Figs. 18d and 18e, the noise levels are almost the same as in the baseline case, with only a $1dB$ noise increase on the retreating side in Fig. 18d. This suggests that deflection-limited actively controlled flaps can be used to reduce vibration without a significant effect on noise, as experimentally observed for HHC and IBC configurations.

Clearly, the dual flap configuration has two advantages. It is more effective in reducing vibrations than the single flap configuration and the vibration reduction it produces is not accompanied by the noise penalty that is present for the single flap configuration. One reason for the lessened noise penalty associated with the dual flap configuration may be attributed to

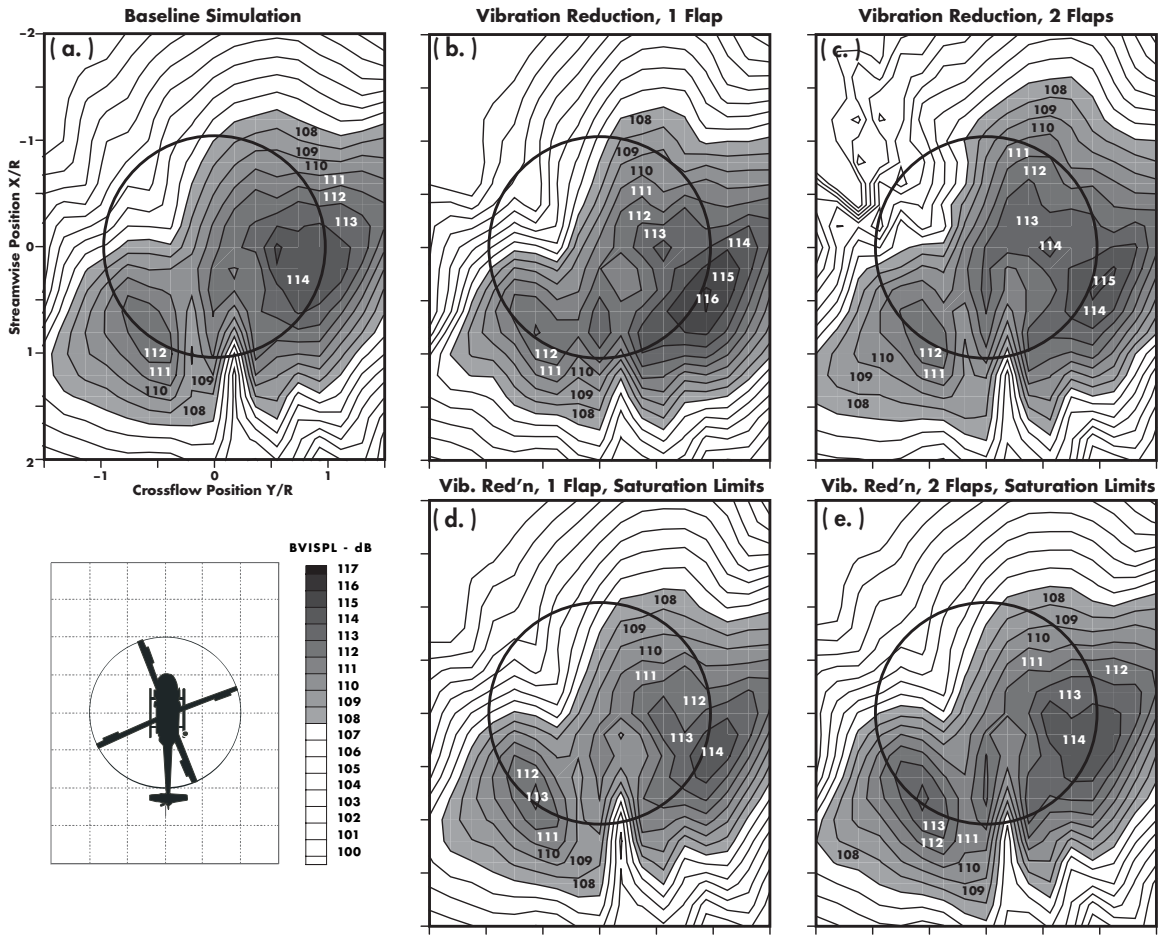


Figure 18: *Increased noise levels for vibration reduction with 1 and 2 flaps, full-scale BO-105*

the smaller flap deflections and the more optimal distribution of the work load between the two flaps.

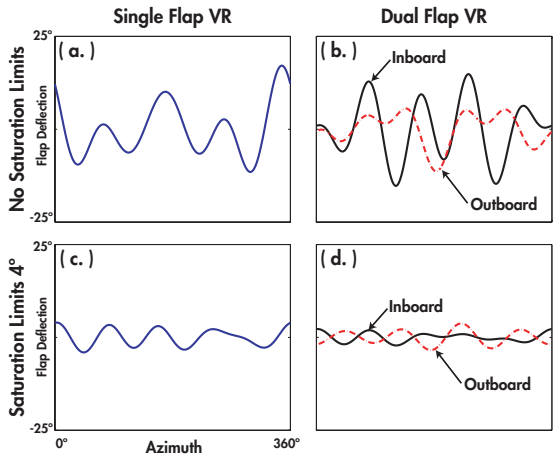


Figure 19: *Flap deflections, vibration reduction*

The deflections of the actively controlled flap over a rotor revolution for the four ACF configurations are shown in Fig. 19(a-d). When saturation limits are not imposed, the single flap configuration can reach flap deflections of almost 20°, shown in Fig. 19a, which exceeds the valid range of the aerodynamic theory used and is unrealistic to implement from a practical point of view. The dual flap configuration (Fig. 19b) shows smaller deflections, peaking at about 18°, however these levels are still an impractical range of flap deflections. When saturation limits are imposed (Figs. 19c and 19d), flap deflections are constrained to remain between $+4°$ and $-4°$. Despite the saturation limits, the dual flap configuration was still very effective at reducing vibration, and produced no noticeable increase in noise beneath the rotor. These results demonstrate that when the controller is not constrained to operate within specified limits on the flap deflections, unrealistic and unnecessarily large flap deflections may be reached.

Vibration Generation During Noise Reduction

First, the conventional HHC control algorithm without saturation limits was used to reduce the noise levels at the SKID1 feedback microphone. The controller could reduce the noise level by $-6dB$ in the single ACF configuration, and by $-9dB$ in the dual ACF configuration. The resulting noise levels on the carpet plane are shown in Fig. 20b for the single ACF and Fig. 20c for the dual ACF. The advancing side noise is decreased by $4-7dB$ but is accompanied by a retreating side noise increase of $1-2dB$. The dual flap configuration was able to reduce the noise level by an additional $3dB$ at the feedback microphone location, but less than $2dB$ difference is visible between single and dual flap configurations on the carpet plane.

Next, the adaptive variant of the HHC controller was implemented for noise reduction using the same feedback microphone SKID1. The adaptive controller was also tested with 4° saturation limits imposed. The noise level at SKID1 was reduced by $8dB$ with a single flap, $12dB$ with two flaps, $5dB$ with a deflection-limited single flap and $6dB$ with a dual flap configuration and saturation limits. The resulting noise levels on the carpet plane are shown in Figs. 21b-21e. All configurations are found to be effective in reducing the advancing side noise on the carpet plane. However increases of $1-2dB$ for these cases are observed on the retreating side. Without saturation limits, reductions of up to $4-8dB$ are achieved on the advancing side, as shown in Figs. 21b and 21c. With deflection limits imposed, the reductions range from $3-5dB$ as shown in Figs. 21d and 21e.

The vibration levels were also monitored during active noise reduction process. When using the conventional HHC algorithm, large vibration increases of $40-100\%$ for the vertical hub shear are observed, as shown in Fig. 22. However, when the adaptive algorithm is used, the vibration penalty is lower, as shown in Fig. 23. In fact, the vertical hub shear is actually reduced for all four adaptive noise reduction cases, although other components increase.

The adaptive HHC algorithm also required smaller flap deflections than the conventional HHC algorithm, as shown in Fig. 24. The single and dual flap configurations with conventional HHC had unrealistic flap deflections of more than 20°, as shown in Figs. 24a and 24b. The adaptive algorithm, however, only required flap deflections of 10°, as shown in Figs. 24c and 24d. When saturation limits were imposed, as indicated in Figs. 24e and 24f, the flap deflections are constrained below 4°.

The adaptive algorithm has a clear advantage over conventional HHC for noise reduction problems. Although the final noise reductions are similar between the two HHC variants, the adaptive algorithm requires smaller flap deflections and has a smaller vibration penalty. This study has suggested that on-line identification can perform a better system identification for the nonlinear flight regime tested. This improved identification can, in turn, result in a better noise reduction without excessive flap deflections. This study has also shown that active noise reduction by means of actively controlled flaps with saturation limits is an effective and practical option. It was noted that all control configurations examined experienced slight retreating side noise increases as the advancing side noise was reduced. This is due to the location of the feedback microphone, SKID1, on the advancing side. This location was chosen to reduce advancing side noise, generally considered to be the most annoying to observers on the ground (Ref. 3). An attempt was made to reduce re-

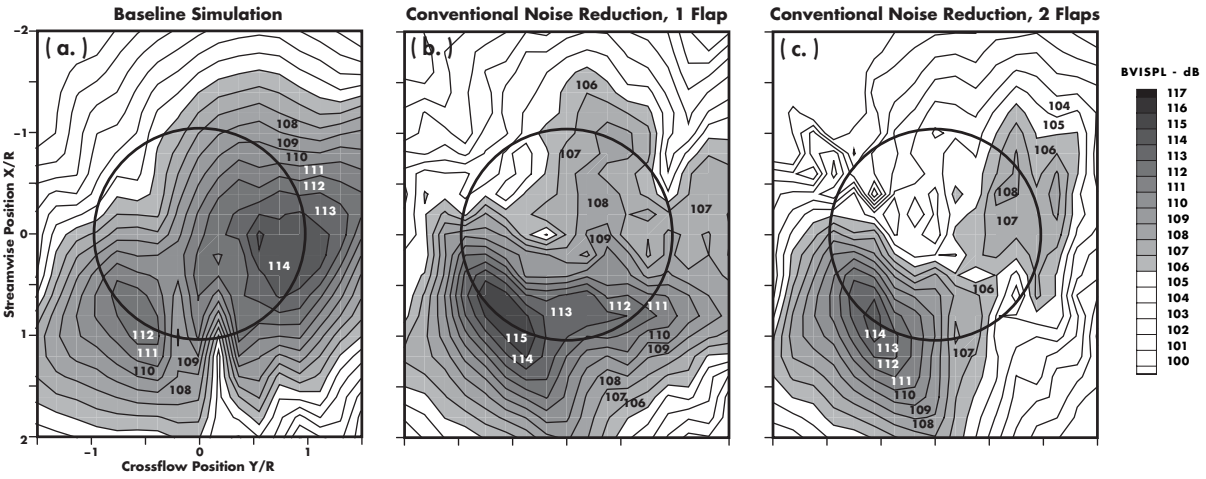


Figure 20: *Noise reduction with 1 and 2 flaps, conventional HHC*

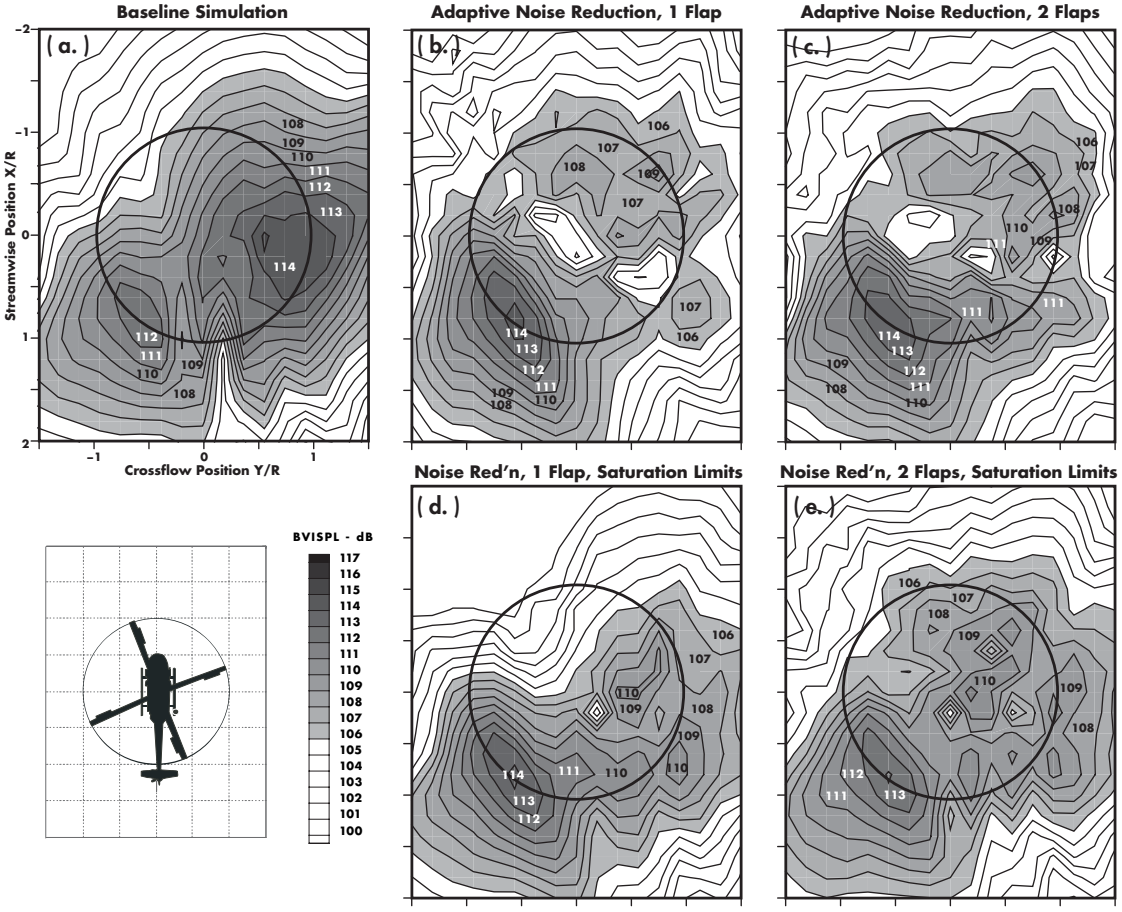


Figure 21: *Noise reduction with 1 and 2 flaps, adaptive HHC*

treating side noise using a microphone on the right skid at the rear, but poor correlation between the feedback microphone and the retreating side noise lobe on the carpet plot. This is probably due to the increased complexity of the noise radiation pattern on the retreating side (Ref. 34).

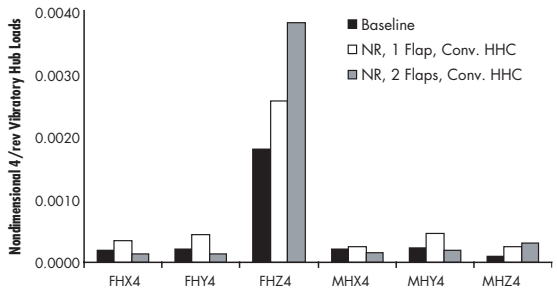


Figure 22: *Vibration levels, noise reduction with 1 and 2 flaps, conventional HHC*

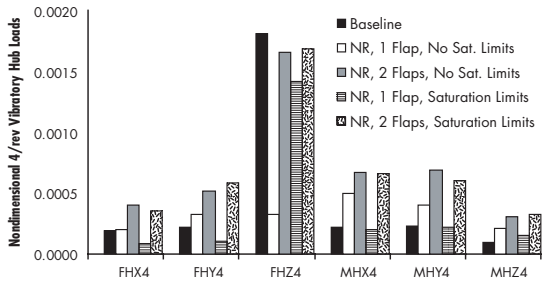


Figure 23: *Vibration levels, noise reduction with 1 and 2 flaps, adaptive HHC*

Simultaneous Vibration and Noise Reduction

Active control using the adaptive HHC algorithm was also implemented for the simultaneous reduction of vibration and noise. Simultaneous reduction was attempted in both single and dual flap ACF configurations, with and without saturation limits. However, when saturation limits were imposed, it was found that the weighting on noise reduction had to be increased in order to obtain useful noise reductions. The diagonal elements of the weighting matrix **Q** (Eq. 3) corresponding to noise weightings were increased by a factor of 10 relative to vibration levels. Reductions in vibration levels were observed for either one or two flaps, as shown in Fig. 25. Without saturation limits imposed, the single ACF could reduce the vertical hub shear by 71%, and the dual ACF by 80%. These reductions of FHZ4 are comparable to the vibration reduction study. However, with saturation limits and the modified control weighting, vibration reductions are 38% and 36% for single and dual flap configurations, respectively.

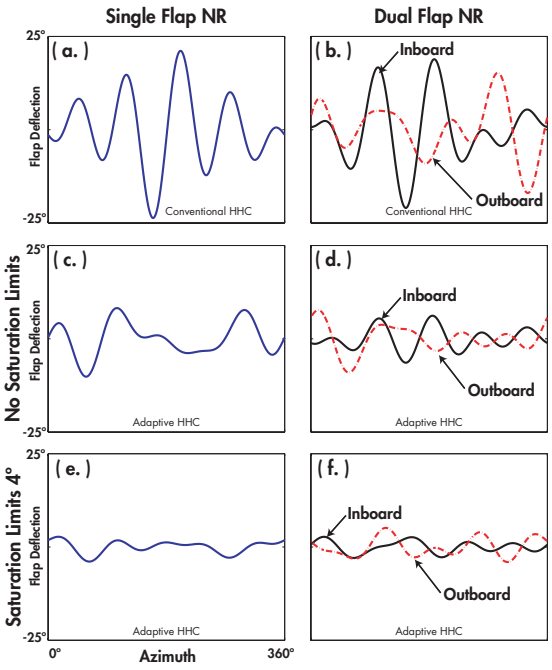


Figure 24: *Flap deflections, noise reduction*

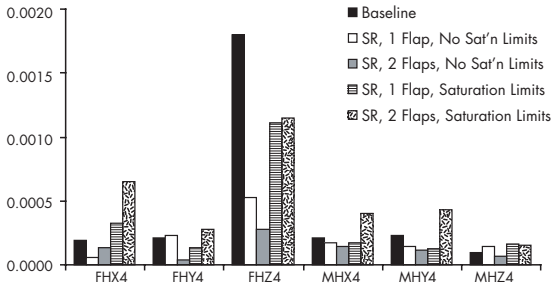


Figure 25: *Vibration levels showing reduction from baseline, simultaneous reduction with 1 and 2 flaps*

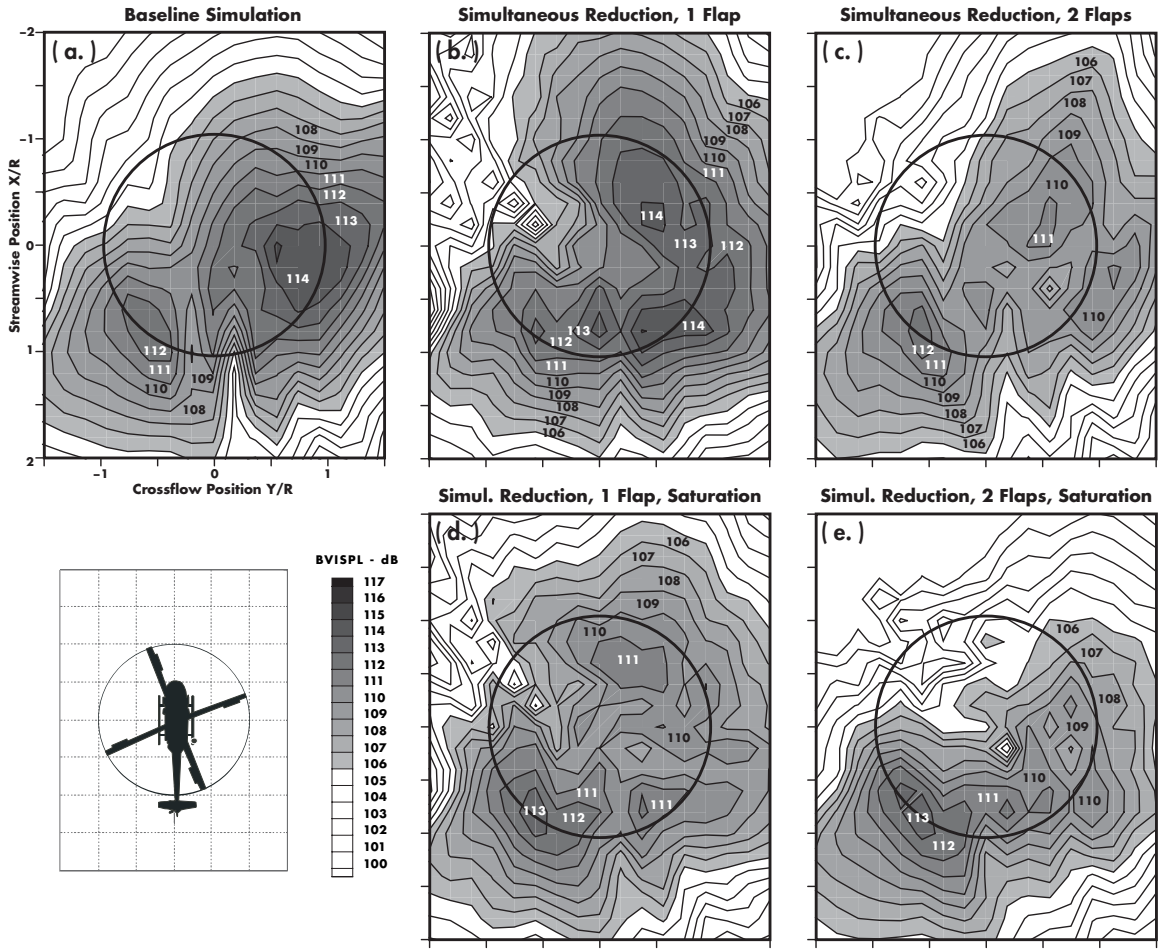


Figure 26: *Noise carpet plot showing reduction from baseline, simultaneous reduction with 1 and 2 flaps*

The noise at the feedback location SKID1 was found to decrease by $2dB$ and $3dB$ for one and two flap configurations without saturation limits, respectively. This is less than the improvement achieved during noise reduction studies, but it represents a significant decrease. With saturation limits and modified weighting, these decreases are $3dB$ and $4dB$ for single and dual flaps, reflecting increased emphasis on noise reduction. The noise levels on the carpet plane are shown in Figs. 26b through 26e. For the single flap case without saturation, in Fig. 26b, no significant noise reduction is observed, although the noise directivity pattern changes somewhat. However, with dual flaps, reductions of $3-5dB$ are found on the advancing side, with no noticeable noise increase on the retreating side, as shown in Fig. 26c. With modified weighting and saturation limits, reductions of $4-5dB$ for the single flap case and $5-6dB$ for the dual flap case are obtained on the retreating side. The improved noise reduction found with saturation limits corresponds to the different weighting matrix used.

The flap deflections for simultaneous noise and vibration reduction are shown in Figs. 27a and 27b for the single and dual ACF setups. With a single flap, deflections are observed to be less than 18°, while the dual ACF setup requires deflections of up to 20°. However, once saturation limits are imposed, deflections remain within the specified 4° limits as shown in Figs. 27c and 27d.

This study has demonstrated that simultaneous active reduction of noise and vibration with actively controlled flaps is feasible. Excellent vibration reduction was achieved, and the dual flap configuration showed noise decreases of up to $5dB$ on the carpet plane, without a retreating side penalty. The flap deflections observed were high when saturation limits were not imposed. However, by changing the weighting $\mathbf{Q}$ and imposing saturation limits, even greater noise reductions of $6dB$ could be achieved, at the expense of a less dramatic reduction of vibration levels.

Changes to Wake Structure

To enhance our understanding of BVI during vibration reduction, the wake and vortex structure for several active control configurations are examined in Fig. 28. Three active control cases, the most effective vibration reduction case, the most effective noise reduction case and the dual flap simultaneous reduction configuration are compared against the baseline rotor wake. Figures 28a-28d present a top-down view of the blade at 35° azimuth, a key position on the advancing side. This case represents the most severe BVI events that contribute to advancing-side noise and vibration. Only the advancing side interactions are considered,

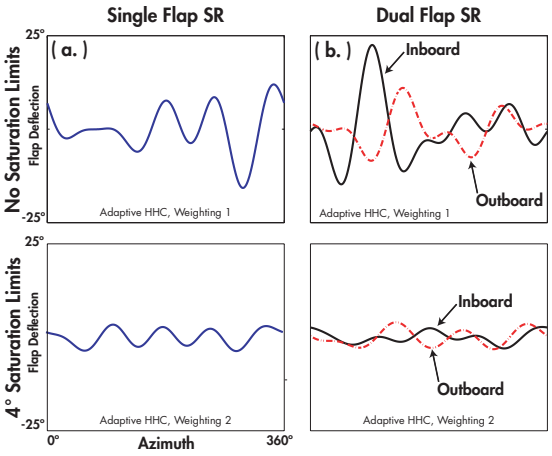


Figure 27: *Flap deflections, simultaneous reduction*

as they are most affected by the active control with a feedback microphone located on SKID1. Figures 28e-28h show the same blade and vortex segments, but in the plane of the rotor, perpendicular to the blade, highlighting the vertical variation of the vortex segments. Figures 28i-28l depict the overall structure of the rotor wake, as seen from the side and also as seen from behind the rotor, looking in the direction of flight. Figures 28m-28o present the nondimensional blade loading $C_N M^2$ as measured at $r/R = 0.87$ along the span of the blade. In these plots, each of the control cases is shown with a dashed line, and the baseline loading pattern is denoted by a solid line.

Several interesting features are evident in these plots. Comparing Fig. 28e (baseline) and 28f (vibration reduction), it is apparent that the miss-distance of the current interaction between the blade and the vortex from blade 3 has changed somewhat from the baseline case. For noise reduction, the a distorted wake pattern is evident in Fig. 28c. This pattern has the effect of reducing the effective length of the blade span subjected to a parallel interaction. Interestingly, Figs. 28d and 28h show an intermediate vortex pattern that contains both of these features, but to a lesser extent.

These computations support experimental and theoretical observations (Ref. 3) suggesting that the BVI interaction angle has an important effect on noise generation. The present study also suggests that compromise wake geometries exist where conditions for reduced noise and vibration can co-exist.

It is apparent that the actively controlled flaps have a distinct and observable effect on the helicopter trailed wake, and thus influence the properties of BVI interactions, aerodynamic loading, vibration levels and noise production.

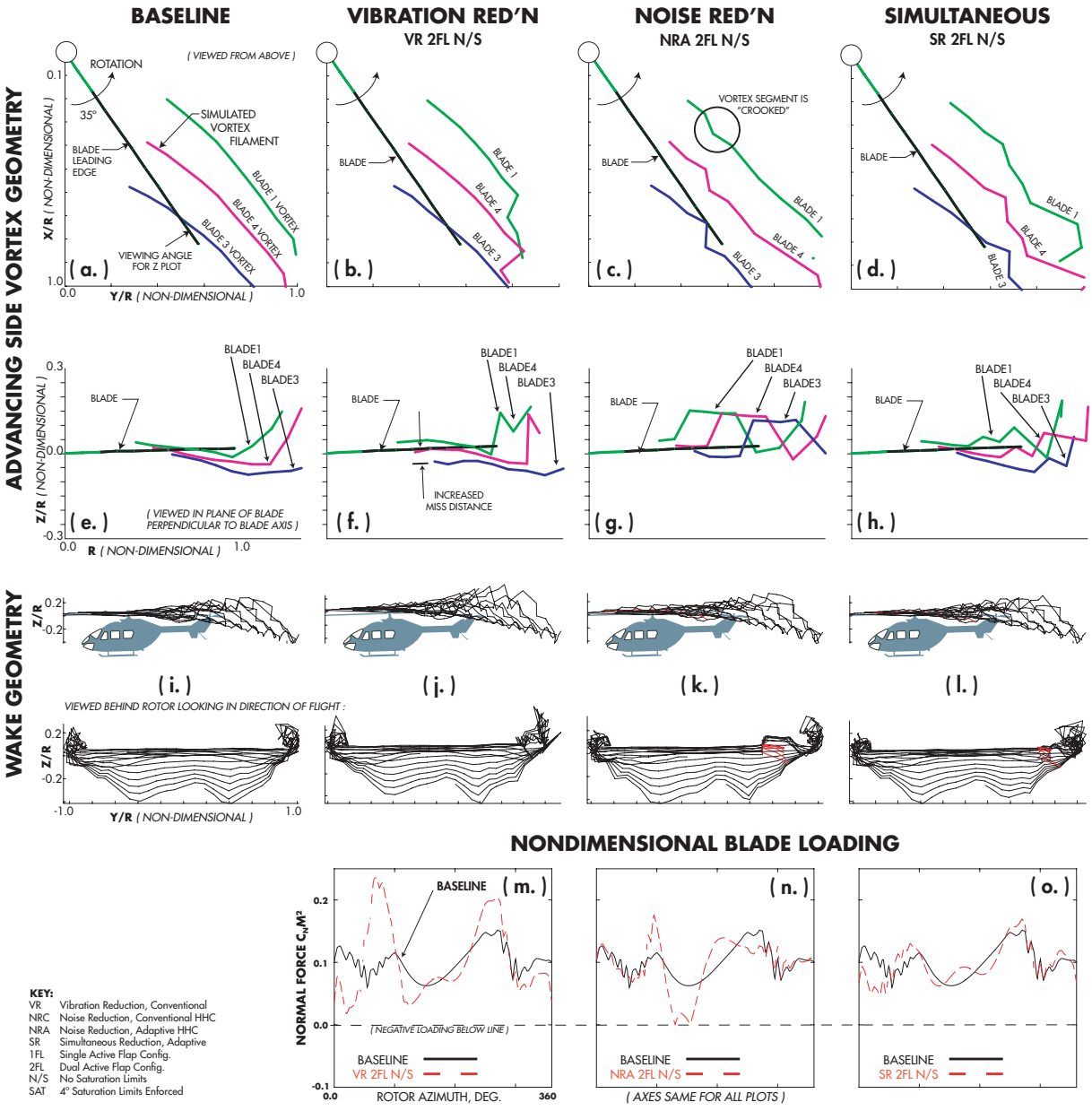


Figure 28: *Changes to wake structure for vibration, noise, and simultaneous reduction with actively controlled flaps*

Rotor and Control System Power Consumption

The control system and rotor power were evaluated for all twelve active control configurations considered, using Eq. 11,

$$P_{cs} = \sum_{k=1}^{N_b=4} \frac{1}{2\pi} \int_0^{2\pi} \left[-M_\delta(\psi_k)\dot{\delta}(\psi_k) \right] d\psi_k. \qquad (11)$$

The control system power as a percentage of rotor power for these cases is presented in Fig. 29. It is evident that the conventional HHC algorithm consumes the most power, largely due to the excessive flap deflections used. When saturation limits are imposed, power requirements are significantly reduced. It is also interesting to note that when using the adaptive algorithm for simultaneous reduction with the dual flap configuration, almost twice the power of adaptive noise reduction with dual flaps is required, but this is essentially the same amount of power required for vibration reduction with dual flaps and the conventional HHC algorithm.

Effect of Active Control on Rotor Trim

An important issue pertaining to the use of an active control device such as actively controlled flaps (ACFs) is how the device will affect helicopter trim. One key advantage of the ACF is that it does not have an adverse effect on helicopter airworthiness. However, it is also possible that flap inputs that achieve optimal vibration or noise suppression might alter the values of trim variables ($\theta_0, \theta_{1c}, \theta_{1s}, \theta_{0t}, \alpha_s, \phi_R$) necessary to maintain steady flight. If the control device requires significant flight control adjustments from the pilot to maintain trimmed flight, the utility of the control device would be compromised. Furthermore, if the controller achieved reductions in noise or vibration by deviating from the desired flight condition, the observed reductions would be artificial.

Previous studies [14,15] have obtained trim and subsequently applied active control to reduce a specific objective. In the present work, this same procedure is executed, but followed by a re-trim, in which the helicopter is retrimmed with optimal control inputs. This is illustrated schematically in Fig. 30.

A number of control configurations have been investigated, using both single and dual flaps, and with and without saturation limits. Using these configurations, the effect of harmonic flap inputs for active control on the rotorcraft trim state will be studied.

Initially, a single flap configuration was used to reduce $4/rev$ vibratory loads in 6° descending flight at $\mu = 0.15$. Results for this configuration are given in

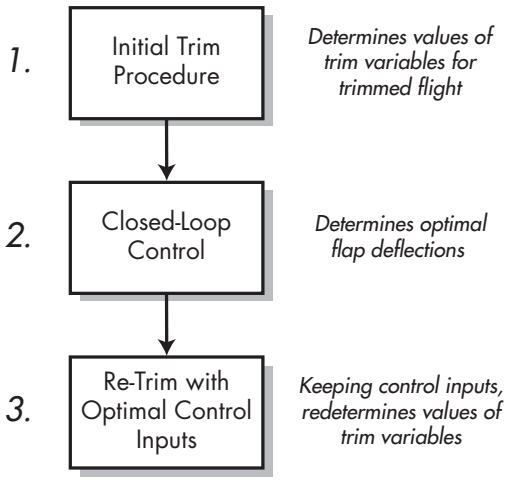


Figure 30: *Procedure for retrimming rotor after active control*

Fig. 31, and show that retrimming the rotor has very little effect on the reduced vibratory loads.

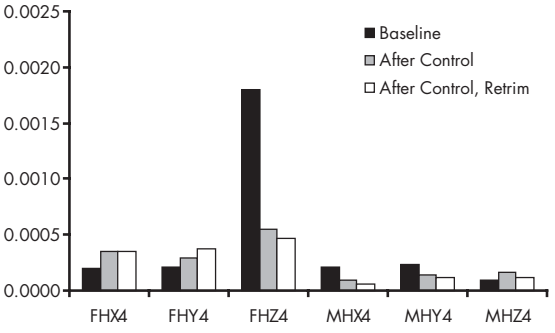


Figure 31: *Results for retrimming rotor, single flap vibration control, no saturation limits, shows little effect on trim*

Additionally, the required pilot inputs for retrimming the rotor were computed, and are shown in Fig. 32. It is apparent that no significant control changes are required to maintain trimmed flight even when the active controller is on.

The flap deflections for this case are shown in Fig. 19a. The flap reaches approximately 18° during the course of a revolution. Despite this relatively large deflection, trim remains essentially unaltered.

Although these results have demonstrated that the active flap controller has negligible effect on trim, several other configurations were also investigated. Reduced vibratory loads corresponding to a dual flap configuration without saturation limits are shown in Fig. 33. Once again, the effect of retrim is shown to be essentially negligible. It should also be noted that when vibratory loads do change after retrim, they do not necessarily increase.

When saturation limits are imposed on a dual flap

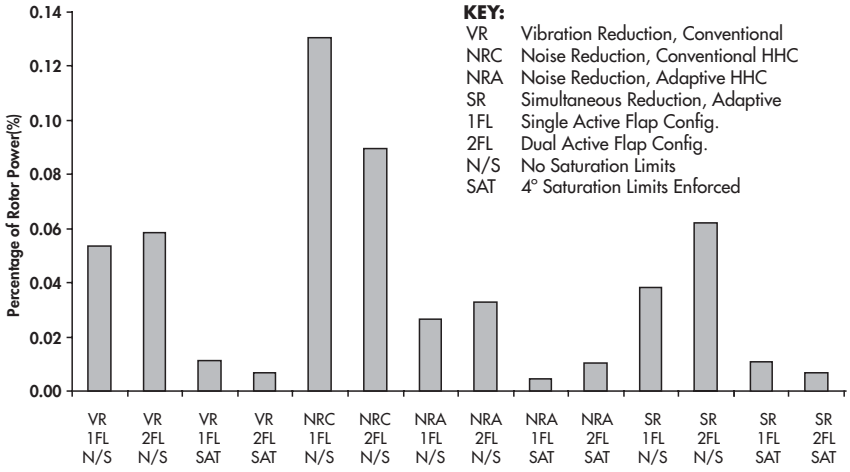


Figure 29: *Control system power as a percentage of rotor power for various configurations*

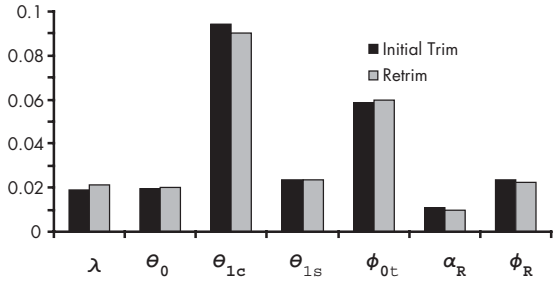


Figure 32: *Only small pilot input are needed to retrim rotor*

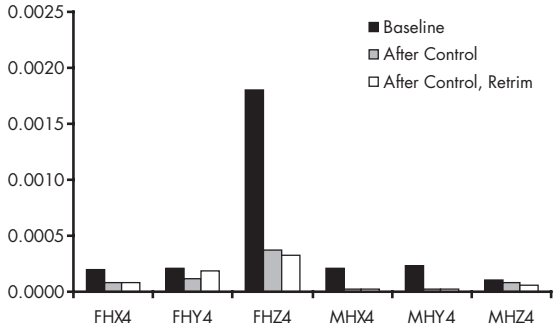


Figure 33: *Results for retrimming rotor, dual flap vibration control, no saturation limits, shows little effect on trim*

configuration, as shown in Fig. 34, the influence on rotor trim is reduced further. Because flap deflections are limited to only 4°, the already small changes to the trim condition are reduced.

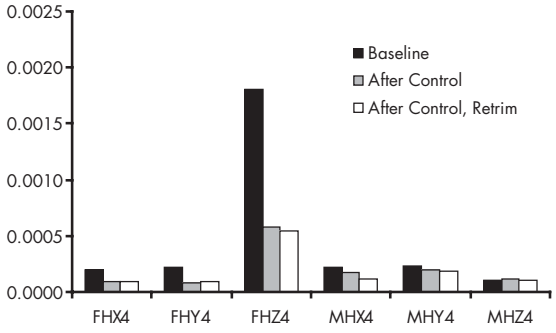


Figure 34: *Results for retrimming rotor, dual flap vibration control, 4° saturation limits, shows little effect on trim*

Finally, the effect of noise reduction was investigated. The controller was used to reduce BVI noise, and subsequently retrimmed. Again, the effect on trim is negligible. Figure 35 shows that vibration levels increase from the baseline, but change very little after retrim.

The effect on noise level is also very small. In the baseline condition, before active control is applied, the measured BVI noise on the right skid is 117.4*dB*. After control, this is reduced to 105.4*dB*, a 12*dB* reduction. Flap deflections of almost 20° are commanded. After control and retrim, the noise level is 105.6*dB*. Thus, the retrim procedure results in a noise increase of 0.2*dB*, an essentially inaudible difference.

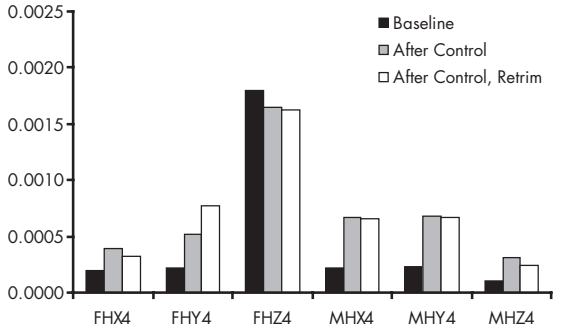


Figure 35: *Results for retrimming rotor, dual flap noise control,* 4° *saturation limits, shows little effect on trim*

Summary and Conclusions

A numerical simulation of noise generation during closed-loop vibration, noise and simultaneous noise and vibration reduction using actively controlled flaps has been conducted. Single and dual ACF configurations were used to reduce $4/rev$ vibrations, and the accompanying noise changes were carefully monitored. The effect of including saturation limits on flap deflections was also considered. Similarly, single and dual ACF configurations were considered for noise reduction, while tracking vibration levels. The conventional and adaptive HHC control algorithms were compared, and saturation limits were also imposed for noise reduction. Finally, simultaneous noise and vibration reduction was achieved, using the adaptive HHC controller with single and dual flap configurations. A summary of the key numerical results of this study is presented in Table 7.

The conclusions that can be drawn from the results presented in this paper are summarized below:

1. The ACF is an effective vibration reduction device for descending flight in the presence of heavy BVI. A dual flap configuration is slightly more effective than a single ACF. Vibration is reduced significantly even in the presence of saturation limits.

2. Noise increases accompany single flap vibration reduction, especially on the advancing side. However, vibration reduction with the dual flap configuration has a substantially smaller adverse effect on noise generation when compared with the single flap configuration. This is associated with both smaller flap angles and optimal workload distribution between the flaps. Imposing saturation limits on a single or dual flap configuration also reduces the associated noise penalty.

3. The ACF may have lessened noise penalties associated with vibration reduction as compared to conventional IBC or HHC.

4. The ACF can be effectively used to reduce advancing-side BVI noise, identified to be most annoying to observers on the ground. The dual flap configuration is more effective than the single flap configuration at reducing noise. Noise reduction is possible even with saturation limits imposed.

5. The adaptive HHC algorithm has a distinct advantage over the conventional HHC algorithm. Smaller flap deflections and less control system power are required and a significantly lessened vibration penalty is encountered.

6. Simultaneous active noise and vibration reduction using the adaptive HHC and a dual ACF configuration is possible. However, it is unlikely that simultaneous reduction can achieve the degree of reduction that isolated vibration or noise reduction can.

7. Specific changes in the wake structure and blade loading are associated with noise, vibration or simultaneous reduction. These computational studies support the finding that the interaction angle heavily influences BVI noise production.

8. Active control implemented by actively controlled trailing edge flap does not significantly affect helicopter trim or flight condition.

Acknowledgments

This research was supported in part by a Rackham Predoctoral Fellowship from the University of Michigan for D. Patt, and by ARO grant 02-1-0202 with Dr. G. Anderson as grant monitor. Partial support by the FXB Center for Rotary and Fixed Wing Air Vehicle Design is also gratefully acknowledged. The authors would also like to thank Dr. Yung H. Yu of the AFDD and Dr. Berend G. van der Wall of the DLR for providing HART test data.

REFERENCES

1. Friedmann, P. P. and Millott, T. A. , "Vibration Reduction in Rotorcraft Using Active Control: A Comparison of Various Approaches," Journal of Guidance, Control, and Dynamics, Vol. 18, (4), July-August 1995, pp. 664–673.

Type	VR	VR	VR	VR	NR	NR	NR	NR	NR	NR	SR	SR	SR	SR
HHC Type	C	C	C	C	C	C	A	A	A	A	A	A	A	A
No. Flaps	1	2	1	2	1	2	1	2	1	2	1	2	1	2
Sat. Limits	–	–	4°	4°	–	–	–	–	4°	4°	–	–	4°	4°
% Δ Vib.†	−69	−79	−35	−68	+43	+111	−82	−9	−22	−7	−71	−85	−38	−36
SKID1 ΔdB	0	1	−1	−1	−6	−9	−8	−12	−6	−5	−2	−3	−3	−4
Power‡	5.4	5.9	1.1	0.66	13	8.9	2.6	3.3	0.44	1.04	3.8	6.2	1.0	0.45

†Change in FHZ4, the vertical $4/rev$ vibratory hub shear. ‡ Value given is the percentage of rotor power used by control system, multiplied by 100.

Table 7: Summary of results for the twelve cases examined

2. Friedmann, P. P. , "Rotary Wing Aeroelasticity - Current Status and Future Trends," Proceedings of the 39th AIAA Aerospace Sciences Meeting and Exhibit, Reno, NV, January 2001. AIAA Paper No. 2001-0427, to be published in the AIAA Journal, September, 2004.

3. Yu, Y. H. , "Rotor Blade-Vortex Interaction Noise," Progress in Aerospace Sciences, Vol. 36, (2), February 2000, pp. 97–115.

4. Friedmann, P. P. , "Vibration Reduction in Rotorcraft Using Actively Controlled Flaps - From Theoretical Concept to Flight-Ready Hardware," Proceedings of the AHS 4th Decennial Aeromechanics Specialist's Conference, San Francisco, CA, January 2004.

5. Brooks, T. F. and Booth, JR, E. R. , "The Effects of Higher Harmonic Control on Blade-Vortex Interaction Noise and Vibration," Journal of the American Helicopter Society, Vol. 38, (3), July 1993, pp. 45–55.

6. Jacklin, S. A. , "Second Test of a Helicopter Individual Blade Control System in the NASA Ames 40 by 80 Foot Wind Tunnel," Proceedings of the 2nd International American Helicopter Society Aeromechanics Specialists Conference, Bridgeport, CT, October 1995.

7. Spletstoesser, W. , Kube, R. , Wagner, W. , Seelhorst, U. , Boutier, A. , Micheli, F. , Mercker, E. , and Pengel, K. , "Key Results From a Higher Harmonic Control Aeroacoustic Rotor Test (HART)," Journal of the American Helicopter Society, Vol. 42, (1), January 1997, pp. 58–78.

8. Kube, R. , van der Wall, B. , Schultz, and Splettstoesser, W. , "IBC Effects on BVI Noise and Vibrations a Combined Numerical and Experimental Investigation," Proceedings of the 55th Annual Forum of the American Helicopter Society, Montreal, Canada, May 1999.

9. Jacklin, S. A. , Haber, A. , de Simone, G. , Norman, T. , Kitaplioglu, C. , and Shinoda, P. , "Full-Scale Wind Tunnel Test of an Individual Blade Control System for a UH-60 Helicopter," Proceedings of the 51st Annual Forum of the American Helicopter Society, Montreal, Canada, June 2002.

10. Booth, E. R. and Wilbur, M. L. , "Acoustic Aspects of Active-Twist Rotor Control," Journal of the American Helicopter Society, Vol. 49, (1), January 2004.

11. Splettstoesser, W. , Seelhorst, U. , Wagner, W. , Boutier, A. , Micheli, F. , Mercker, E. , and Pengel, K. , "Higher Harmonic Control Aeroacoustic Rotor Test (HART) - Test Documentation and Representative Results," DLR Report IB 129-95/28 and appendices, December 1995.

12. Lim, C. , Tung, C. , Yu, Y. , Burley, C. , Brooks, T. F. , Boyd, D. , van der Wall, B. G. , Schneider, O. , Richard, P. , Beaumier, P. , Delrieux, Y. , and Pengel, K. , "Hart-II: Prediction of Blade-Vortex Interaction Loading," Proceedings of the 29th Europen Rotorcraft Forum, Friedrichschafen, Germany, September 2003.

13. Malovrh, B. and Gandhi, F. , "Localized Individual Pitch Control for Reduction of Helicopter Blade-Vortex Interaction Noise," Proceedings of the 28th European Rotorcraft Forum, Bristol, England, September 2002, pp. 6.1–6.10.

14. Patt, D. , Liu, L. , and Friedmann, P. P. , "Rotorcraft Vibration Reduction and Noise Prediction Using a Unified Aeroelastic Response Simulation," Proceedings of the 59th American Helicopter Society Annual Forum, Phoenix, AZ, May 2003.

15. Liu, L. , Patt, D. , and Friedmann, P. P. , "Active Vibration and Noise Reduction in Rotorcraft Using an Aeroelastic Simulation," Proceedings of the American Helicopter Society 4th Decennial Specialists Conference on Aeromechanics, San Francisco, CA, Jan 2004.

16. de Terlizzi, M. and Friedmann, P. P. , "Active Control of BVI Induced Vibrations Using a Refined Aerodynamic Model and Experimental Correlation," Proceedings of the 51st Annual Forum of the American Helicopter Society, Fort Worth, TX, May 1995, pp. 510–524.

17. Depailler, G. and Friedmann, P. P. , "Reductions of Vibrations Due to Dynamic Stall in Helicopters Using an Actively Controlled Flap," Proceedings of the 43rd AIAA/ASME/ASCE/AHS/ACS Structures, Structural Dynamics and Materials Conference, Denver, CO, April 2002.

18. Cribbs, R. , "Vibration Reduction in Helicopters Using Active Control of Structural Response (ACSR) with Improved Aerodynamic Modeling," Ph.D. Dissertation, University of California, Los Angeles, 1999.

19. Myrtle, T. F. and Friedmann, P. P. , "Application of a New Compressible Time Domain Aerodynamic Model to Vibration Reduction in Helicopters Using an Actively Controlled Flap," Journal of the American Helicopter Society, Vol. 46, (1), January 2001, pp. 32–43.

20. Friedmann, P. P. , de Terlizzi, M. , and Myrtle, T. F. , "New Developments in Vibration Reduction with Actively Controlled Trailing Edge Flaps," Mathematical and Computer Modelling, Vol. 33, 2001, pp. 1055–1083.

21. Johnson, W. , CAMRAD/JA - A Comprehensive Analytical Model of Rotorcraft Aerodynamics and Dynamics, Vol I. Theory Manual. Johnson Aeronautics, Palo Alto, CA, 1988.

22. Johnson, W. , CAMRAD/JA - A Comprehensive Analytical Model of Rotorcraft Aerodynamics and Dynamics, Vol II. Users' Manual. Johnson Aeronautics, Palo Alto, CA, 1988.

23. Scully, M. P. , "Computation of Helicopter Rotor Wake Geometry and its Influence on Rotor Harmonic Airloads," Ph.D. Dissertation, Aeroelastic Research Laboratory, Massachusetts Institute of Technology, 1975.

24. Rahier, G. and Delrieux, Y. , "Blade-Vortex Interaction Noise Prediction Using a Rotor Wake Roll-Up Model," Journal of Aircraft, Vol. 34, (4), Jul.-Aug. 1997, pp. 522–530.

25. Tauszig, L. , "Analysis of Helicopter Blade-Vortex Interaction Noise With Application to Adaptive-Passive and Active Alleviation Methods," Ph.D. Dissertation, The Pennsylvania State University, 2002.

26. Patt, D. , Liu, L. , Chandrasekar, J. , Bernstein, D. S. , and Friedmann, P. P. , "The HHC Algorithm for Helicopter Vibration Reduction Revisited," Proceedings of the 45th AIAA/ASME/ASCE/AHS/ACS Structures, Structural Dynamics and Materials Conference, Palm Springs, CA, April 2004. AIAA Paper No. 2004-1948.

27. Johnson, W. , Self-Tuning Regulators for Multicyclic Control of Helicopter Vibrations. NASA Technical Paper 1996, 1982.

28. Cribbs, R. and Friedmann, P. P. , "Actuator Saturation and Its influence on Vibration Reduction by Actively Controlled Flaps," AIAA Paper No. 2001-1467. Proceedings of the 42nd AIAA/ASME/ASCE/AHS/ACS Structures, Structural Dynamics and Materials Conference, Seattle, WA, April 2001.

29. Millott, T. A. and Friedmann, P. P. , Vibration Reduction in Helicopter Rotors Using an Actively Controlled Partial Span Trailing Edge Flap Located on the Blade. NASA CR 4611, June 1994.

30. Kube, R. , Splettstoesser, W. , Wagner, W. , Seelhorst, U. , Yu, Y. H. , Tung, C. , Beamier, P. , Prieur, J. , Rahier, G. , Spiegel, P. , Boutier, A. , Brooks, T. F. , Burley, C. L. , Boyd, D. D. , Mercker, E. , and Pengel, K. , "HHC Aeroacoustic Rotor Tests in the German-Dutch Wind Tunnel: Improving Physical Understanding and prediction results," Aerospace Science and Technology, Vol. 2, (3), March 1998, pp. 177–190.

31. Wachspress, D. A. and Quackenbush, T. R. , "BVI Noise Prediction Using a Comprehensive Rotorcraft Analysis," Proceedings of the American Helicopter Society 57th Annual Forum, Washington, DC, May 2001.

32. Beaumier, P. and Spiegl, P. , "Validation of ONERA Aeroacoustic Prediction Methods for Blade-Vortex Interaction Using HART Test Results," Proceedings of the 51st Annual Forum of the American Helicopter Society, Fort Worth, TX, May 1995, pp. 510–524.

33. DuVall, T. , Sim, B. W. , and Schmitz, F. H. , "Cabin versus Far-Field Blade-Vortex Interaction Noise Level Trends," Proceedings of the American Helicopter Society Aerodynamics, Acoustics and Test Evaluation Technical Specialists Meeting, San Francisco, CA, January 2002.

34. Schmitz, F. H. and Sim, B. W. , “Blade-Vortex Interaction (BVI) Noise: Retreating Side Characteristics, Sensetivity to Chordwise Loading and Unsteady Aerodynamics,” Proceedings of the AHS Aeromechanics Specialists Meeting, Atlanta, GA, November 2000.